RSC Advances

ROYAL SOCIETY OF CHEMISTRY

www.rsc.org/advances

Acid-induced formation of hydrogen-bonded double helix based on chiral polyphenyl-bridged bis(2,2'-bipyridine) ligands

Kiu-Chor Sham, Chi-Chung Yee, Yi Pan, Kai-Chung Lau, Shek-Man Yiu, Hoi-Lun Kwong*

Department of Biology and Chemistry, City University of Hong Kong, Tat Chee Avenue, Kowloon, Hong Kong SAR (China) Fax: 852 3442 0522; Tel: 852 3442 7304; E-mail: bhhoik@cityu.edu.hk

Abstract

A series of chiral polyphenyl-bridged bis(2,2'-bipyridine) ligands comprising one to four phenyl units were synthesized. The ligands give a weak signal in the CD spectra, but upon addition of tetrachloroferric acid or perchloric acid, a more intense CD signal is observed for ligands having two or more phenyl units. Titration experiments show that the CD signal comes from a monoprotonated species which give broadened and upfielded ^{1}H NMR signals. Variable temperature NMR experiments split the broadened signals into two sets of signals when the temperature is decreased. One of the set is remarkably upfield while the others has chemical shift similar to that of the free ligand. The X-ray crystal structures of a free ligand (mono phenyl), a monoprotoned ligand (biphenyl) and a biprotonated ligand (tetraphenyl) were obtained and the structure of the monoprotoned ligand shows that it is a double-stranded helix, which is stabilized by interior hydrogen bonding between the pyridinium N$^+$H and the pyridine N of another ligand strand, and exterior CH$\cdots$Cl hydrogen bonding between $FeCl_4^-$ and the two ligand strands. Theoretical DFT calculations show that there is such stabilization in solution as well. With perchlorate anion, the helix formation process is reversible with Et_3N which accompanies with an on/off CD signal change.

Introduction

Double helix is ubiquitous in biological molecules and its sophisticated structure is often closely related to its biological function.[1] Inspired by nature, chemists have great interest to prepare artificial molecules with double helical structure.[2–8] Self-assembly is the most commonly used approach in which non-covalent interactions, such as electrostatic,[9,10] metal-ligand,[7,8,11–16] π–π stacking[17–19] and hydrogen bonding,[20–24] drive the two strands to intertwine in the formation process. These interactions of the two strands can come from motifs that are incorporated into the strands during synthesis[20] or from a third component, like metal ion, which

induces the interactions.[7,8]

Important to both biological and chemical process,[25,26] anions can form hydrogen-bond and this hydrogen-bonding interaction has been shown to play curial role in the formation of many supramolecular system[27,28] which include double helices.[29–32] In the double helix examples, chloride, fluoride or sulfate, are locate at the helical axis, and form multiple strong N–H···Cl, N–H···F and N–H···O hydrogen bonds, respectively, to both ligand strands to stabilize the double helices.

Proton, the smallest cation, can interact with the lone pair electron of a ligand strand and lead to hydrogen bonds. Huc et al.[33] and Aida et al.[34] have both reported the use of proton to induced formation of single-stranded helices, however, to the best of our knowledge, double helix formation induced by proton is not known. We have previously reported the synthesis of Mn double-stranded helicates with mono- to tri-phenyl-bridged bis(2,2'-bipyridine) **L1**–**3** ligands.[35] Herein, together with a tetraphenyl-bridged bis(2,2'-bipyridine) **L4,** we report the synthesis of this series of ligands. Upon protonation, ligands **L2**–**4** give intense CD signal in the presence of $FeCl_4^-$ or ClO_4^- anion. CD and NMR titration experiments suggest that a monoprontonated ligand species is responsible for the intense CD signals and X-ray crystal structures of monoprotonated **L2** shows that a double-stranded helix is responsible for the signal.

Experimental

Chemicals and Starting Materials

Solvents used for synthesis were of analytical grade. All starting chemicals were of reagent-grade quality and were obtained commercially and used as received without further purification. Synthesis of chiral bromobipyridine **1** was reported previously.[36]

Physical Measurements and Instrumentation

^{1}H, COSY and NOESY NMR spectra were recorded on Bruker 400 MHz instrument. The ^{1}H and chemical shift was referred to TMS as reference. Electrospray (ESI) mass spectra were measured by a PE SCIEX API 150 EX system. CD spectra were recorded on a Biokin MOS-450 instrument with a 1 mm cell.

Crystal Structure Determination.

For crystal structure of **L1**, data was collected at 293 K with an Oxford Diffraction Gemini S Ultra X-ray single crystal diffractometer using graphite monochromatized Mo-Kα radiation (λ = 0.71073 Å). For structure of $[(\mathbf{L2})_2H_2](ClO_4)_2$ and $[(\mathbf{L4})H_2(Cl)](FeCl_4)$, data were collected at 133 K with an

Oxford Diffraction Gemini S Ultra X-ray single crystal diffractometer using graphite monochromatized Cu-Kα radiation (λ = 1.54178 Å). All collected frames were processed with the software SAINT, and absorption correction was applied (SAD-ABS) to the collected reflections. The structure of the complex was solved by direct methods (SHELXTL) in conjunction with standard difference Fourier syntheses. All non-hydrogen atoms were assigned with anisotropic displacement parameters. The hydrogen atoms were generated in their idealized positions and allowed to ride on the respective carbon atoms. Crystal data of **L1**. $C_{80}H_{76}N_8O$, M = 1165.49, orthorhombic, a = 10.0224(4), b = 13.5194(6), c = 24.219(1) Å, U = 3281.6(2) Å^3, space group $P2_12_12_1$, Z = 4, 10071 reflections measured, 5493 unique (R_{int} = 0.0228) which were used in all calculation. The final $wR(F_2)$ was 0.0804 (all data). Crystal data of [(**L2**)$_2$H$_2$](FeCl$_4$)$_2$. $C_{96}H_{94}Cl_8Fe_2N_8O_{1.75}$, M = 1783.09, monoclinic, a = 30.7135(9), b = 21.8661(6), c = 15.6061(5) Å, U = 10290.2(5) Å^3, space group $C2$, Z = 4, 24178 reflections measured, 14245 unique (R_{int} = 0.0346) which were used in all calculation. The final final $wR(F_2)$ was 0.1416 (all data). Crystal data of [(**L2**)$_2$H$_2$](FeCl$_4$)$_2$. $C_{96}H_{94}Cl_8Fe_2N_8O_{1.75}$, M = 1783.09, monoclinic, a = 30.7135(9), b = 21.8661(6), c = 15.6061(5) Å, U = 10290.2(5) Å^3, space group $C2$, Z = 4, 24178 reflections measured, 14245 unique (R_{int} = 0.0346) which were used in all calculation. The final final $wR(F_2)$ was 0.1416 (all data). Crystal data of [(**L4**)H$_2$](Cl)(FeCl$_4$). $C_{59}H_{56}Cl_5FeN_4O$, M = 1070.18, monoclinic, a = 11.4756(3), b = 17.6487(5), c = 26.0159(7) Å, U = 5182.0(2) Å^3, space group $C12_11$, Z = 4, 12966reflections measured, 9565 unique (R_{int} = 0.0259) which were used in all calculation. The final final $wR(F_2)$ was 0.099 (all data). CCDC 983706-983708

DFT calculations

All calculations were done at M06-2X (hybrid meta exchange-correlation functional with double the amount of nonlocal exchange) functional[37] using LanL2DZ basis set for Fe,[38–40] 6-31G(d) basis sets for H, C, N, and 6-31+G(d) basis sets for O, Cl atoms. The solvent effect is taken account by the Polarizable Continuum Model.[41,42] Atom-in-molecule (AIM) analysis is performed with AIM2000 program.[43] The wavefunction was taken from the optimized structure at the M06-2X level with using LanL2DZ basis set for Fe and 6-31G(d) basis set for all non-metal elements.

Procedure for synthesis of 2 and 3

A solution of **1** (1.45 mmol) and tetrakis(triphenylphospine)palladium(0) (0.06 mmol) in degased toluene (6 ml) was treated with a solution of sodium carbonate (2.0 mmol) in H_2O (3 ml). A methanolic solution (3 ml) of 3-chlorophenylboronic acid (1.45 mmol) or 3-bromophenylboronic acid (1.19 mmol) was added. The mixture was

stirred at 80 ^{o}C for 3 h under nitrogen. After cooling to room temperature, aqueous NH_3 (30 ml) was added and the mixture was extracted by CH_2Cl_2. The combined organic layers were dried by $MgSO_4$. Solvent was removed under reduced pressure. The crude product was purified by column chromatography (petroleum ether:ethyl acetate = 10:1). Products were isolated as white solid in 95% and 83% yield for **2** and **3**, respectively. ^{1}H NMR of **2** (300 MHz, $CDCl_3$) δ 8.94 (d, *J* = 7.8 Hz, 1H), 8.60 (s, 1H), 8.49 (s, 1H), 8.05 (m, 2H), 7.95 (m, 1H), 7.85 (d, *J* = 8 Hz, 1H), 7.42 (m, 2H), 3.29 (d, *J* = 2.4 Hz, 2H), 3.02 (t, *J* = 5.4 Hz, 1H), 2.8 (m, 1H), 2.41 (s, 1H), 1.43 (s, 3H), 1.23 (d, *J* = 10.3 Hz, 1H), 0.64 (s, 3H). ^{1}H NMR of **3** (300 MHz, CD_2Cl_2): δ 8.37 (s, 1H), 8.35 (d, 1H, *J* = 8.1 Hz), 8.31 (t, 1H, *J* = 1.8 Hz), 8.22 (s, 1H), 8.02 (d, 1H, *J* = 7.8 Hz), 7.85 (t, 1H, *J* = 7.8 Hz), 7.67 (d, 1H, 6.9 Hz), 7.55 (d, 1H, *J* = 7.8 Hz), 7.36 (t, 1H, *J* = 7.8 Hz), 3.10 (d, 1H, *J* = 2.7 Hz), 2.88 (t, 1H, *J* = 5.4 Hz), 2.70 (m, 1H), 2.33 (m, 1H), 1.42 (s, 3H), 1.21 (d, 1H, *J* = 6.9 Hz), 0.67 (s, 3H).

Procedure for synthesis of 4

A solution of **3** (11.6 mmol) and tetrakis(triphenylphospine)palladium(0) (5 mol%) in degased toluene (36 ml) was treated with a solution of sodium carbonate (20 mmol) in H_2O (16.5 ml). A methanolic solution (16.5 ml) of 3-chlorophenylboronic acid (11.6 mmol) was added. The mixture was stirred at 95 ^{o}C for 24 h under nitrogen. After cooling to room temperature, aqueous NH_3 (50 ml) was added and the mixture was extracted by CH_2Cl_2. The combined organic layers were dried by $MgSO_4$. Solvent was removed under reduced pressure. The crude product was purified by column chromatography (petroleum ether:ethyl acetate = 10:1). Products were isolated as white solid with 93% yield. ^{1}H NMR (400 MHz, $CDCl_3$) δ 8.56 (d, *J* = 7.8 Hz, 1H), 8.49 (s, 1H), 8.33 (s, 1H), 8.29 (t, *J* = 1.5 Hz, 1H), 8.16 (d, *J* = 7.3 Hz, 1H), 7.98 (t, *J* = 7.8 Hz, 1H), 7.85 (d, *J* = 7.2 Hz, 1H), 7.70 (t, *J* = 1.7 Hz, 1H), 7.66 (d, *J* = 7.7 Hz, 1H), 7.63 (d, *J* = 7.6 Hz, 1H), 7.59 (d, *J* = 7.6 Hz, 1H), 7.43 (t, *J* = 7.7 Hz, 1H), 7.38 (d, *J* = 8.0 Hz, 1H), 3.18 (d, *J* = 2.5 Hz, 2H), 2.96 (t, *J* = 5.4 Hz, 1H), 2.8 (m, 1H), 2.4 (m, 1H), 1.46 (s, 3H), 1.27 (t, *J* = 8.2 Hz, 1H), 0.69 (s, 3H).

Procedure for synthesis of L1 and L3

Degas toluene (16 ml), MeOH (6 ml) and water (6 ml) were added to a flask containing $Pd(PPh_3)_4$ (0.17 g, 3 mol%), **1** or **3** (4.4 mmol), 1,3-phenyldiboronic acid (0.34 g, 2 mmol) and sodium carbonate (0.92 g). The mixture was heated at 80 ^{o}C for 24 h. It was cooled to room temperature. Ammonia solution in saturated Na_2CO_3 solution was added and the solution was stirred for 5 min. It was extracted by CH_2Cl_2. Solvent was dried under vacuo, and the compound was purified by column chromatograph with solvent (dichloromethane : diethyl ether = 10 : 1). The crude

yellow solution can be further purified by washing with MeCN. Products were isolated as pale yellow solid with 57% and 30% yield for **L1** and **L2**, respectively. ^{1}H NMR of **L1** (400 MHz, $CDCl_3$): δ 8.81 (t, 1H, *J* = 1.6 Hz), 8.85 (s, 2H), 8.38 (d, 2H, *J* = 6.7 Hz), 8.27 (d, 2H, *J* = 7.8 Hz), 8.25 (s, 2H), 7.93 (t, 2H, *J* = 7.7 Hz), 7.87 (d, 2H, *J* = 6.8 Hz), 7.69 (t, 1H, *J* = 7.7 Hz) 3.11 (d, 4H, *J* = 2.6 Hz), 2.90 (t, 2H, *J* = 5.4 Hz), 2.73 (m, 2H), 2.34 (m, 2H), 1.44 (s, 6H), 1.27 (d, 2H, *J* = 9.6 Hz), 0.69 (s, 6H). ^{13}C NMR ($CDCl_3$): δ 156.65, 156.61, 154.86, 145.68, 145.57, 143.30, 140.30, 140.36, 137.86, 129.38, 127.93, 125.80, 120.90, 120.42, 119.50, 44.82, 40.38, 39.54, 33.30, 32.08, 26.28, 21.66. ^{1}H NMR of **L3** (300 MHz, $CDCl_3$): δ 8.43 (m, 4H), 8.36 (d, 2H, *J* = 6 Hz), 8.22 (s, 2H), 8.16 (d, 2H, *J* = 6 Hz), 8.05 (t, 1H, *J* = 1.8 Hz), 7.90 (t, 2H, *J* = 7.8 Hz), 7.81 (d, 2H, *J* = 7.8 Hz), 7.75 (t, 4H, *J* = 7.5 Hz), 7.63 (t, 3H, *J* = 7.5 Hz), 3.05 (d, 4H, *J* = 2.7 Hz), 2.88 (t, 2H, *J* = 5.4 Hz), 2.70 (m, 2H), 2.30 (m, 2H), 1.41 (s, 6H), 1.21 (d, 2H, *J* = 6.9 Hz), 0.65 (s, 6H). ^{13}C NMR ($CDCl_3$): δ 156.62, 156.54, 154.75, 145.65, 145.58, 143.31, 142.15, 141.91, 140.53, 137.87, 129.52, 129.43, 128.09, 126.67, 126.44, 126.26, 120.88, 120.35, 119.48, 44.80, 40.37, 39.49, 33.23, 32.06, 26.25, 21.63.

Procedure for synthesis of L2

To a solution of $NiCl_2 \cdot 6H_2O$ (1.2 mmol) in degassed DMF (15 ml) at 70 ^{o}C under nitrogen, triphenylphosphine (4.8 mmol) was added to give a blue solution. Zinc powder (2.6 mmol) was then added and the resulting mixture was stirred for an hour, in which dark-brown mixture was formed. **2** (1 mmol) in degassed DMF (5 ml) was added slowly and the mixture stirred at 70 ^{o}C for 72 hours. The mixture was then allowed to cool to room temperature and 25% aqueous NH_3 (25 ml) was added. The layers were separated, and the aqueous layers were extracted with CH_2Cl_2. The solution was dried with $MgSO_4$ and solvent was removed under reduced pressure. Crude product was purified by column chromatography. Product was isolated as a pale yellow solid. Yield: 37%. ^{1}H NMR of **L2** (300 MHz, $CDCl_3$): δ 8.43 (m, 2H), 8.37 (d, 2H, *J* = 7.5 Hz), 8.22 (s, 1H), 8.18 (d, 1H, *J* = 8.1 Hz), 7.90 (t, 1H, *J* = 7.8 Hz), 7.83 (d, 1H, *J* = 7.2 Hz), 7.78 (d, 1H, *J* = 7.8 Hz), 7.64 (t, 1H, *J* = 7.5 Hz), 3.05 (d, 2H, *J* = 2.7 Hz), 2.88 (t, 1H, *J* = 5.4 Hz), 2.70 (m ,1H), 2.31 (m, 1H), 1.42 (s, 3H), 1.21 (d, 1H, *J* = 6.9 Hz), 0.66 (s, 3H). ^{13}C NMR ($CDCl_3$): δ 156.43, 156.38, 154.63, 145.46, 145.39, 143.11, 140.13, 137.68, 129.18, 127.73, 125.57, 120.70, 120.23, 119.28, 44.56, 40.12, 39.30, 33.07, 31.85, 26.05, 21.44.

Procedure for synthesis of L4

To a solution of $NiCl_2 \cdot 6H_2O$ (3.8 mmol) in degassed DMF (17 ml) at 70 ^{o}C under nitrogen, triphenylphosphine (16 mmol) was added to give a blue solution. Zinc

powder (6.4 mmol) was then added and the resulting mixture was stirred for an hour, in which dark-brown mixture was formed. Compound **4** (3.2 mmol) in degassed DMF (9 ml) was added slowly and the mixture stirred at 70 ^{o}C for 72 hours. The mixture was then allowed to cool to room temperature and 25% aqueous NH_3 (100 ml) was added. The layers were separated, and the organic layers were washed with CH_2Cl_2. The solution was dried with $MgSO_4$ and solvent was removed under reduced pressure. Crude product was purified by column chromatography (dichloromethane : n-hexane : diethyl ether = 30 : 6 : 1). Product was isolated as a pale brown solid in 26% yield. ^{1}H NMR (400 MHz, $CDCl_3$) δ 8.42 (d, *J* = 2.8 Hz, 1H), 8.37 (d, *J* = 7.6 Hz, 1H), 8.22 (s, 1H), 8.16 (d, *J* = 7.3 Hz, 1H), 8.02 (s, 1H), 7.90 (t, *J* = 7.8 Hz, 1H), 7.80 (d, *J* = 7.7 Hz, 1H), 7.74 (t, *J* = 7.2 Hz, 2H), 7.62 (d, *J* = 13.8, 7.6 Hz), 3.06 (d, *J* = 2.3 Hz, 1H), 2.89 (t, *J* = 5.4 Hz, 1H), 2.7 (m, 1H), 2.32 (s, 1H), 1.43 (s, 2H), 1.25 (d, *J* = 9.8 Hz, 1H), 0.67 (s, 2H). ^{13}C NMR ($CDCl_3$): δ 156.40, 156.33, 254.57, 145.46, 125.40, 143.12, 141.98, 141.84, 141.65, 140.31, 137.71, 129.28, 127.90, 126.54, 126.43, 126.30, 126.05, 120.72, 120.19, 119.33, 44.57, 40.14, 39.28, 33.02, 31.87, 23.06, 21.45.

Procedure for reversibility experiment

To a solution of **L** (**L2–4**, 3×10^{-4} M in CH_2Cl_2) in a 3 mm cell, 1 equiv. of $HClO_4$ was added, and the CD spectrum of the solution was obtained. After that, 1.2 equiv. of NEt_3 was added to the above solution to fully restore the original spectrum. The experiments were repeated by following the sequence, and the absorption at 334 nm which is the maximum of the induced CD signals was plotted.

Results and discussion

Synthesis of polyphenyl-bridged bis(2,2'-bipyridine) ligands

Chiral polyphenyl-bridged bis(2,2'-bipyridine) ligands **L1–4** with pinene-based chiral substituents at the 4,5-postion of terminal pyridine rings were prepared from bipyridine intermediate **1**, which was obtained from reported Kröhnke condensation between of pyridinium iodide and *α,β*-unsaturated ketone.[36] The Pd-catalyzed Suzuki coupling between **1** and *m*-phenylenediboronic acid with Na_2CO_3 in a mixture of H_2O, MeOH and toluene yielded the monophenyl-bridged **L1** in 57% yield. For the synthesis of biphenyl-bridged **L2**, Pd-catalyzed Suzuki coupling between **1** and 3-chlorophenylboronic acid resulted in the chlorophenylbipyridine intermediate **2**. Ni(0)-mediated homocoupling of **2** in DMF gave **L2** in 37% yield. For the synthesis of triphenyl-bridged **L3**, the reaction between **2** and *m*-phenylenediboronic acid with $Pd(PPh_3)_4$ as catalyst was first tried, but no reaction was observed. Then,

bromophenylbipyridine intermediate **3**, prepared by Pd-catalyzed Suzuki coupling between **1** and 3-bromophenylboronic acid, was employed. A sub-stoichiometric amount of 3-bromophenylboronic acid was used to reduce the formation of the bromobiphenylbipyridine and Suzuki coupling between **3** and *m*-phenylenediboronic acid yielded **L3** in 30% yield. For the synthesis of tetraphenyl-bridged **L4**, intermediate **4**, synthesized by the reaction between **3** and 3-chlorophenylboronic acid with $Pd(PPh_3)_4$ as catalyst, was used. Ni(0)-mediated homocoupling of **4** yielded **L4** in 26% yield.

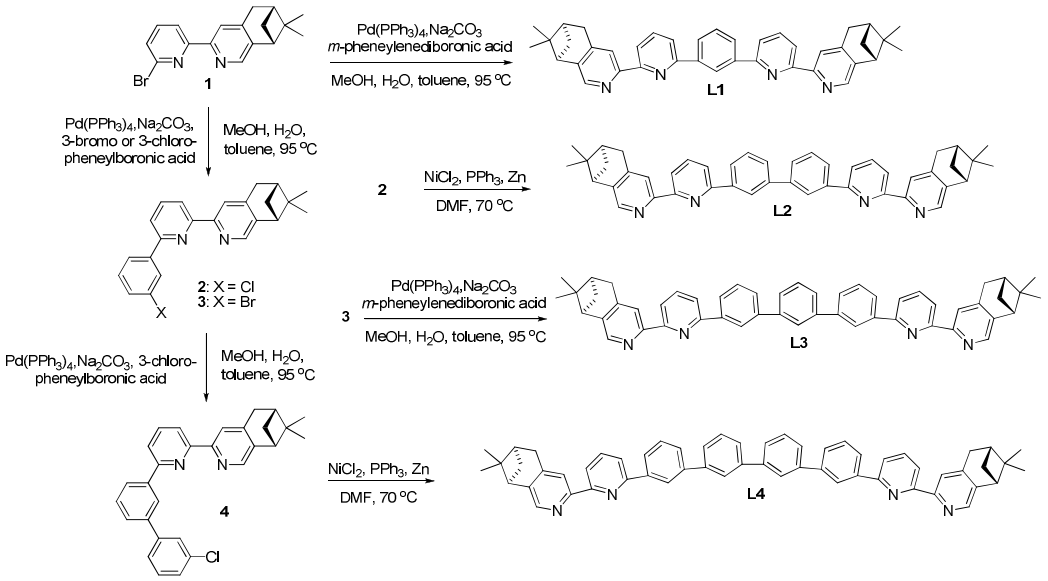

Scheme 1 Preparation of polyphenyl-bridged bis(2,2'-bipyridine) **L1–4**

Effect of acid on the CD spectra of polyphenyl-bridged bis(2,2'-bipyridine) ligands

Although **L1–4** contains chiral substitution at the 4,5-position of the terminal pyridine rings, they gave only a weak CD absorption. Figure 1a–d show the effect of different acids on the CD spectrum of the ligands. The phenyl-bridged **L1** does not show much effect with addition of acid. Only very small change in the CD spectrum of **L1** is observed (Figure 1a). However, **L2–4** show much greater change with addition of some acid. Figure 1b shows the results obtained with the biphenyl-bridged **L2**. Addition of $HFeCl_4$ gives an intense induced CD signal absorption at 334 nm with $\Delta\varepsilon = 6.0\ M^{-1}cm^{-1}$.[44] $HClO_4$ and HOTf give similar change but with weaker intensity, $\Delta\varepsilon = 4.0$ and $2.0\ M^{-1}cm^{-1}$, respectively. Figure 1c shows the results obtained with the triphenyl-bridged **L3**. Similar to the results of **L2**, addition of $HFeCl_4$, $HClO_4$ and HOTf to **L3** leads to induced CD signals at 333 nm with $\Delta\varepsilon$ = 10.2, 4.3, and 3.0 $M^{-1}cm^{-1}$, respectively. These signals have larger intensity when compared to **L2**.

Figure 1d shows the results obtained with the tetraphenyl-bridged **L4**. Intense induced CD signals with $\Delta\varepsilon$ = 9.0, 5.0, and 1.7 $M^{-1}cm^{-1}$ are observed at 330 nm with addition of $HFeCl_4$, $HClO_4$ and HOTf, respectively, which are comparable to **L3**. The trend of $HFeCl_4$ giving the strongest absorption, followed by $HClO_4$ and then HOTf, is very similar to **L2** and **L3**. With the additions of acids other than $HFeCl_4$, $HClO_4$ and HOTf, the CD spectra of **L2**–**4** give very minimal change.

When comparing the polyphenyl-bridged ligands, much stronger acid-induced CD spectral change are observed with **L2**–**4** than **L1** and it seems to suggest that **L2**–**4** give similar species upon protonation. For **L2**–**4**, the CD signal change does not seem to follow the trend of the pK_a value; for example, $HClO_4$ (pK_a = −10.0) give a more intense signal than HOTf (pK_a = −14.0). Other acids like HOAc (pK_a = −4.8), HCl (pK_a = −8.0), HNO_3 (pK_a = −1.3), H_2SO_4 (pK_a = −3.0) give only very small or no CD change. These results suggest that the CD signal change is not triggered by protonation alone. Anion seems to have a role in the change of the CD signal as well.

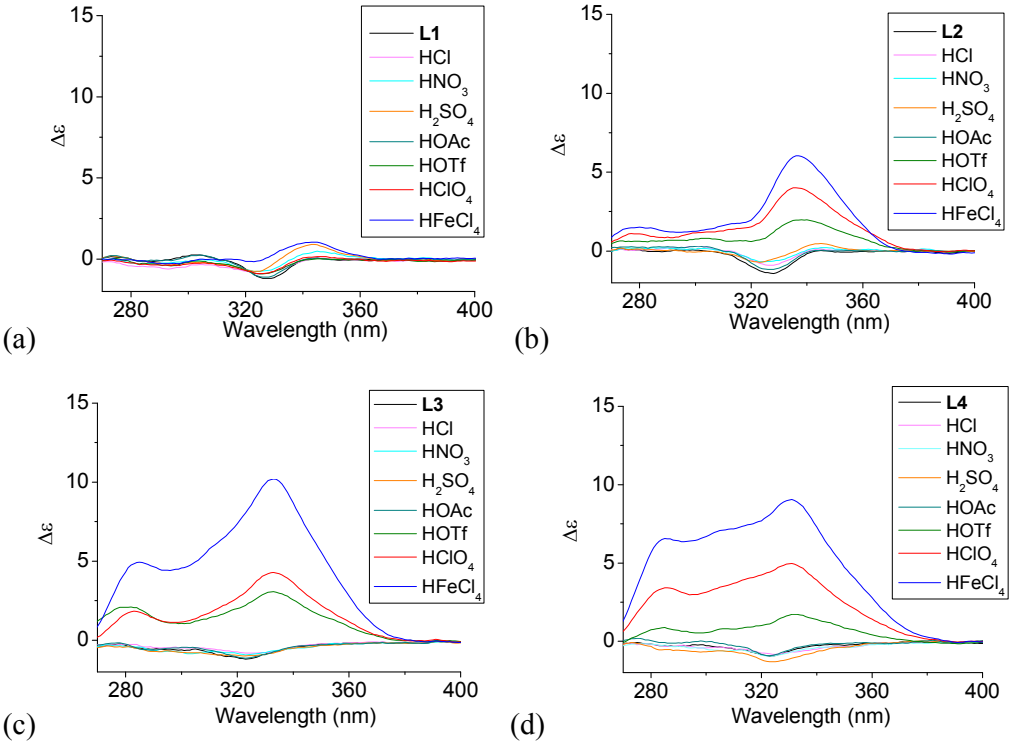

Figure 1 CD spectra of **L1**–**4** (3×10^{-4} M) with addition of different acids (1 equiv).

ESI-MS study

With $HFeCl_4$ giving the largest CD signals, the ESI-MS spectra of the ligands with 1 equiv. of $HFeCl_4$ were obtained for **L1**–**4** (3×10^{-4} M). The spectrum with **L1** is shown in figure 2a. The spectrum show peaks at m/z 575.8 and 1151.6, which can

be assigned to $[(\mathbf{L1})H]^+$ and $[(\mathbf{L1})_2H]^+$, respectively, indicating protonation of **L1** by $HFeCl_4$. Figure 2b shows the spectrum with **L2**. Similar to **L1**, peaks corresponding to $[(\mathbf{L2})H]^+$ and $[(\mathbf{L2})_2H]^+$ are observed, however, in addition to these peaks, a peak at 1500.8 which can be assigned to $[(\mathbf{L2})_2H_2](FeCl_4)^+$ is also observed. This formula indicates that a dimeric form of monoprotonated **L2** may have been formed. The spectrum with **L3**, which is shown in figure 2c, has peaks at m/z 729.1, 1452.4 which corresponds to $[(\mathbf{L3})H]^+$ and $[(\mathbf{L3})_2H]^+$, respectively. Again, the spectrum of **L3** shows peak corresponded to a dimeric species, $[(\mathbf{L3})_2H_2](FeCl_4)^+$, at 1654.3. For **L4**, the spectrum show peaks corresponded to $[(\mathbf{L4})H]^+$, $[(\mathbf{L4})_2H]^+$, and $[(\mathbf{L4})_2H_2](FeCl_4)^+$ at m/z 805.7, 1606.4, and 1806.5 respectively (figure 2d). The signals of $[(\mathbf{L})_2H_2](FeCl_4)^+$ (**L = L2–4**) observed in the spectra suggest the presences of dimeric species $[(\mathbf{L})_2H_2](FeCl_4)_2$, but this species is not observed with **L1**.

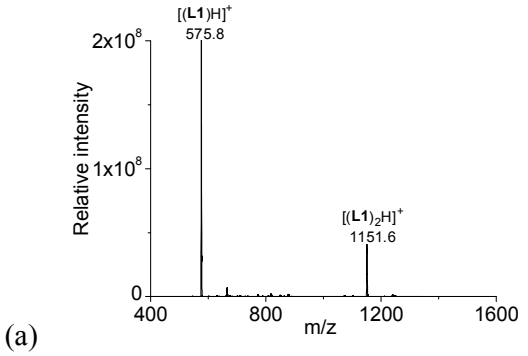

(a)

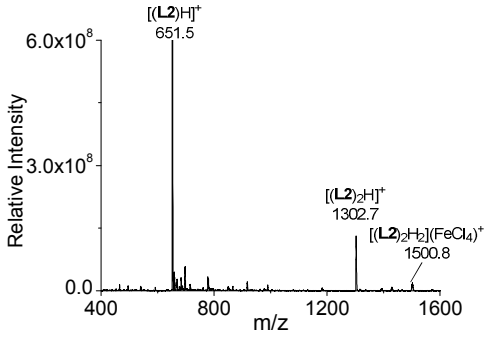

(b)

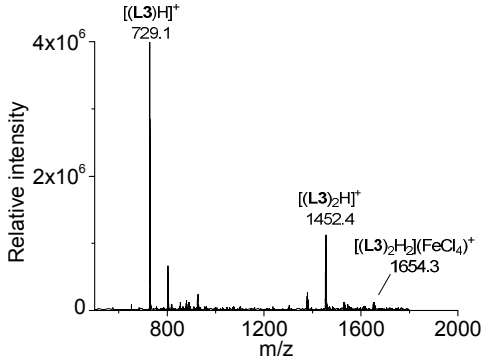

(c)

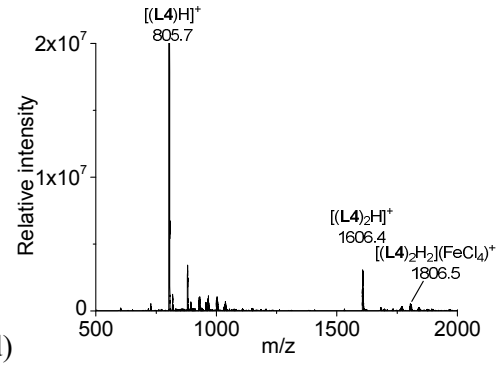

(d)

Figure 2 ESI-MS spectrum of a CH_2Cl_2 solution of **L1**–**4** with addition of $HFeCl_4$.

Acid titration monitored by CD

In order to have a better understanding of the change in CD signals, titration experiments were carried out. As shown in figure 3, addition of various concentration of $HFeCl_4$ into a 3×10^{-4} M solution of **L2** first give positive absorption, then decrease in absorption. The inset shows the change in intensity of the absorption at 334 nm. The intensity of the signal reaches maximum when there is 1 equiv. of $HFeCl_4$. Further addition decreases the signal intensity, and finally the positive CD absorption completely disappeared when 3 equiv. of $HFeCl_4$ is added. A similar trend in the change of CD signals was also observed in the titration experiments of **L3** and **L4**. Figure 4 and 5 show the change of the intensity of the CD signals with concentration of $HFeCl_4$. The signal reach maximum when there is 1 equiv. of $HFeCl_4$, and the intensity of signal decreases with further increase of $HFeCl_4$. These titration experiments suggest that the CD signals are originated from a monoprotonated state, and the acid-induced signal is lost upon further protonation.

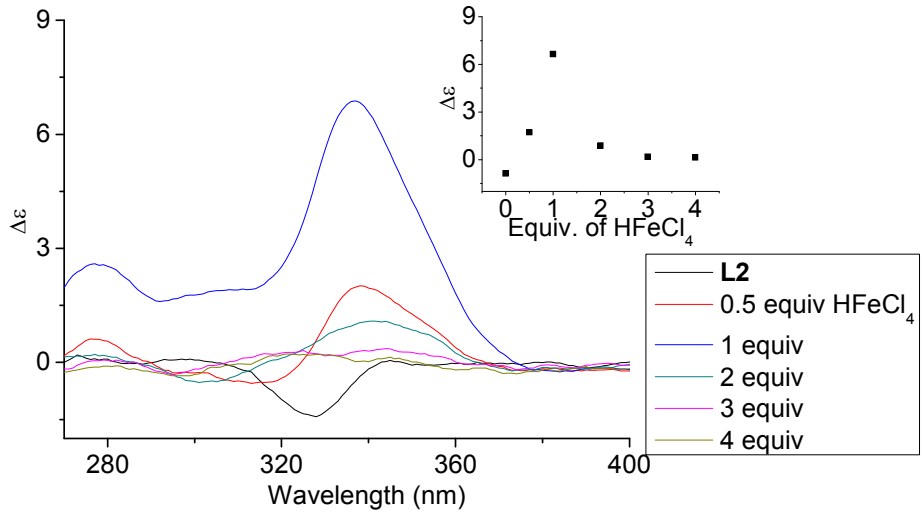

Figure 3 CD spectrum of **L2** (3×10^{-4} M) in CH_2Cl_2 with addition of $HFeCl_4$ (0 to 4 equiv). The inset shows the change in absorption at 334 nm.

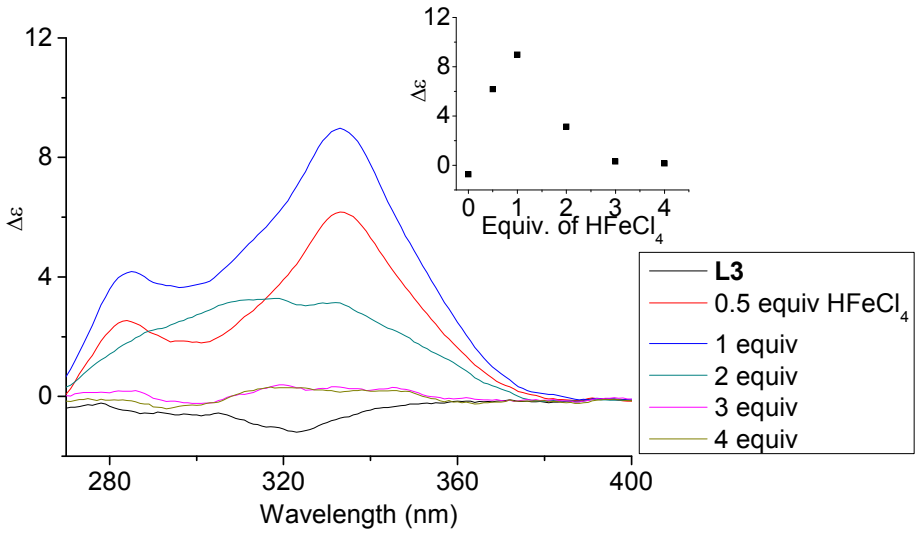

Figure 4 CD spectrum of **L3** in CH_2Cl_2 (3×10^{-4} M) with addition of $HFeCl_4$ (0 to 4 equiv). The inset shows the change in absorption at 333 nm.

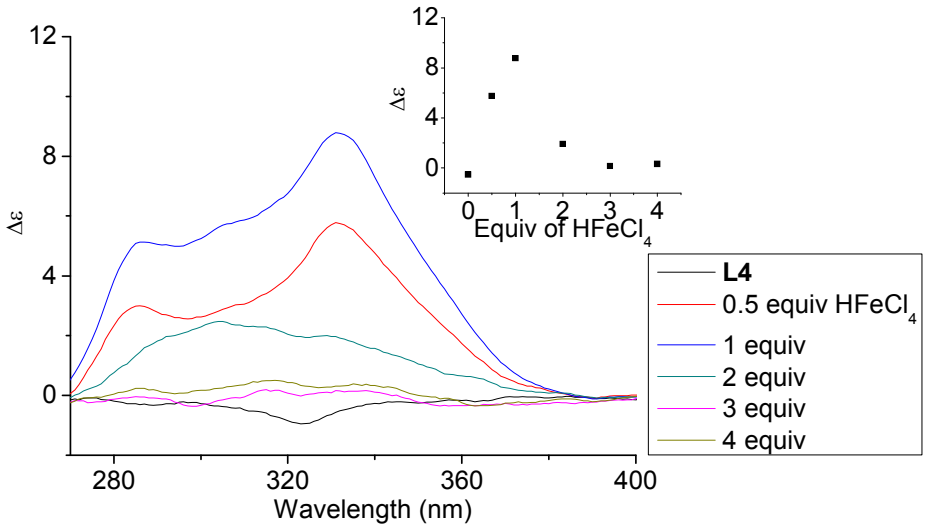

Figure 5 CD spectrum of **L4** in CH_2Cl_2 (3×10^{-4} M) with addition of $HFeCl_4$ (0 to 4 equiv). The inset shows the change in absorption at 332 nm.

Acid titration monitored by NMR

With the paramagnetic nature of $HFeCl_4$, NMR informations were obtained by using $HClO_4$. With **L2**–**4**, titration experiments were carried out under the same concentration as the CD experiments. Figure 6 shows the results with **L2**. With addition of $HClO_4$, there is an immediate upfield shift and broadening of the ^1H NMR signals. The most upfield and broadened signals appear when 2 equiv. of $HClO_4$ is added. Further addition of $HClO_4$ leads to a downfield shift and sharpening of the signals. Sharpened signals with chemical shift similar to the unprotonated **L2** is obtained when more acid is added. However, unlike CD titration where the concentration is limited, the NMR titration can be carried out at a much higher concentration. Figure 7 shows the spectra when the experiment is carried out at 2×10^{-2} M of **L2**, only 1 equiv. of $HClO_4$ is needed to lead to the upfield signals. Figure 8 and 9 are the spectra of titrations with **L3** and **L4** which also show similar change, but in both of this case only one equiv. of $HClO_4$ is needed for reaching the most upfield signal at the CD experiments concentration. These results suggest that the upfield signals may come from the monoprotonation of the polyphenyl-bridged bis(2,2'-bipyridine) ligands. By considering that the induced CD signals and the upfield ^1H signals occurred at the same time, we believe that they come from the same protonated species.

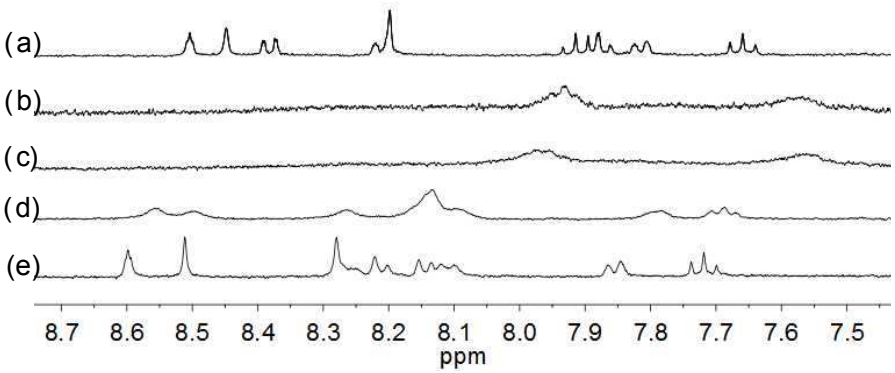

Figure 6 ^{1}H NMR spectra (400 MHz) of (a) **L2** (3×10^{-4} M) in CD_2Cl_2 with addition of (b) 1 equiv (c) 2 equiv (d) 3 equiv (e) 4 equiv of $HClO_4$

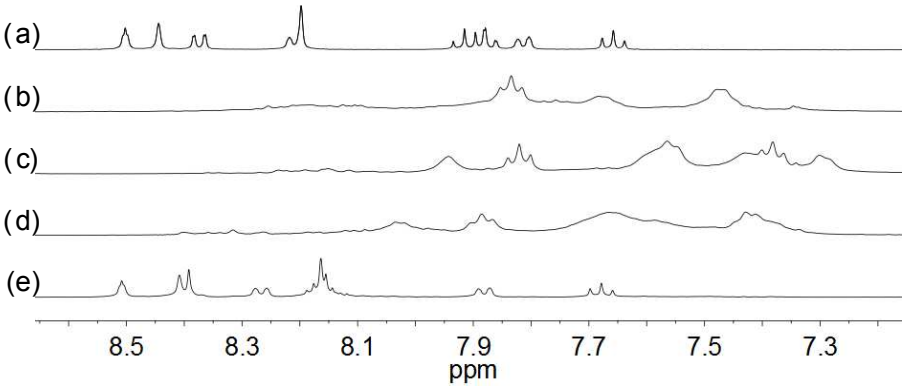

Figure 7 ^{1}H NMR spectra for (a) **L2** (2×10^{-2} M) in CD_2Cl_2 with addition of (b) 0.5 equiv (c) 1.0 equiv (d) 1.5 equiv (e) 2.0 equiv of $HClO_4$.

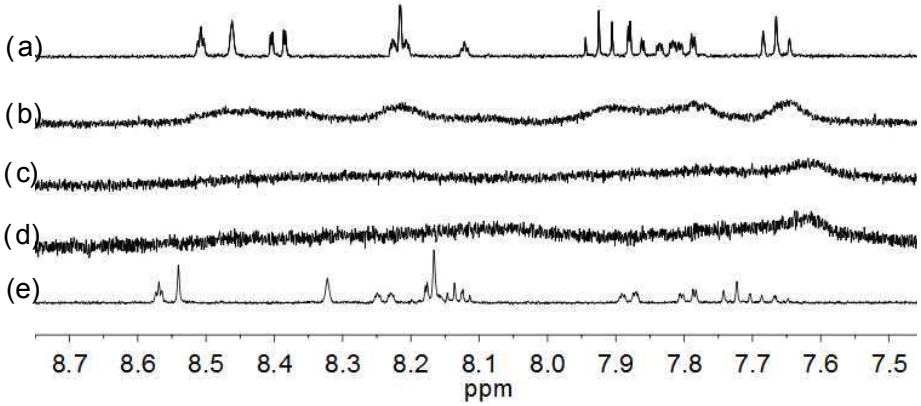

Figure 8 ^{1}H NMR spectra for (a) **L3** (3×10^{-4} M) in CD_2Cl_2 with addition of (b) 0.5 equiv (c) 1 equiv (d) 2 equiv (e) 3 equiv of $HClO_4$.

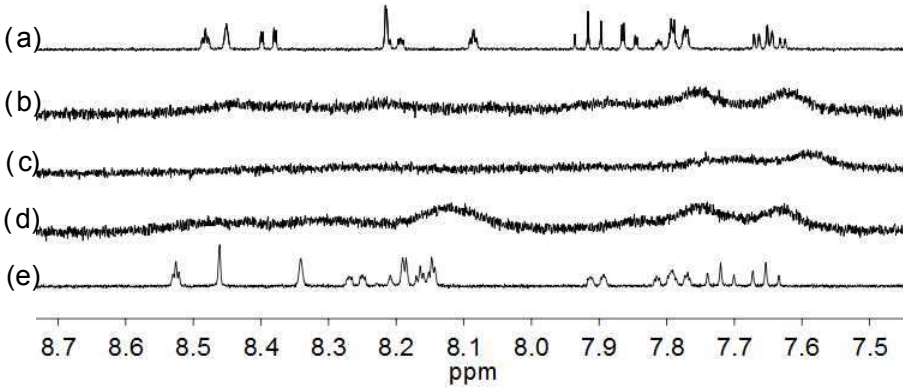

Figure 9 ^{1}H NMR spectra for (a) **L4** (3×10^{-4} M) in CD_2Cl_2 with addition of (b) 0.5 equiv (c) 1 equiv (d) 2 equiv (e) 3 equiv of $HClO_4$.

^{1}H NMR assignment

To have a better understanding of the species, 2D NMR was carried out. The NOESY spectrum of **L2** is shown in figure 10. The correlation signals between the pyridine proton H^5 and both protons at the 2- and 6-position of the bridging phenyl ring, H^6 and H^9, suggests that **L2** interconverts between two conformations with H^5 syn either to H^6 or H^9. Although broadened signals observed with addition of 1 equiv. of $HClO_4$ cannot be assigned, the sharpened signals observed at 2 equiv. of $HClO_4$ were fully assigned. The *syn*-conformation of the mono-protonated 2,2'-bipyridine is well established by both x-ray crystal structure and theoretical calculation.[45,46] The correlation signal between H^2 and H^3 observed in the NOESY spectrum (figure 11) suggests that the pyridyl rings of both bipyridine units are in *syn*-conformation which is consistence with the mono-protonation of the bipyridine units. By considering that proton at the 2-position of the phenyl ring, H^9, gives correlation signals to both protons at the 4-position of the phenyl ring, H^8, and the 5'-position of the bipyridine, H^5, a biprotonated species with a linear conformation is proposed. This biprotonated species comes from the further protonation of the species giving the upfield signals, which is consistent with the suggestion that the upfield signal is most likely a monoprotonated species of **L2**.

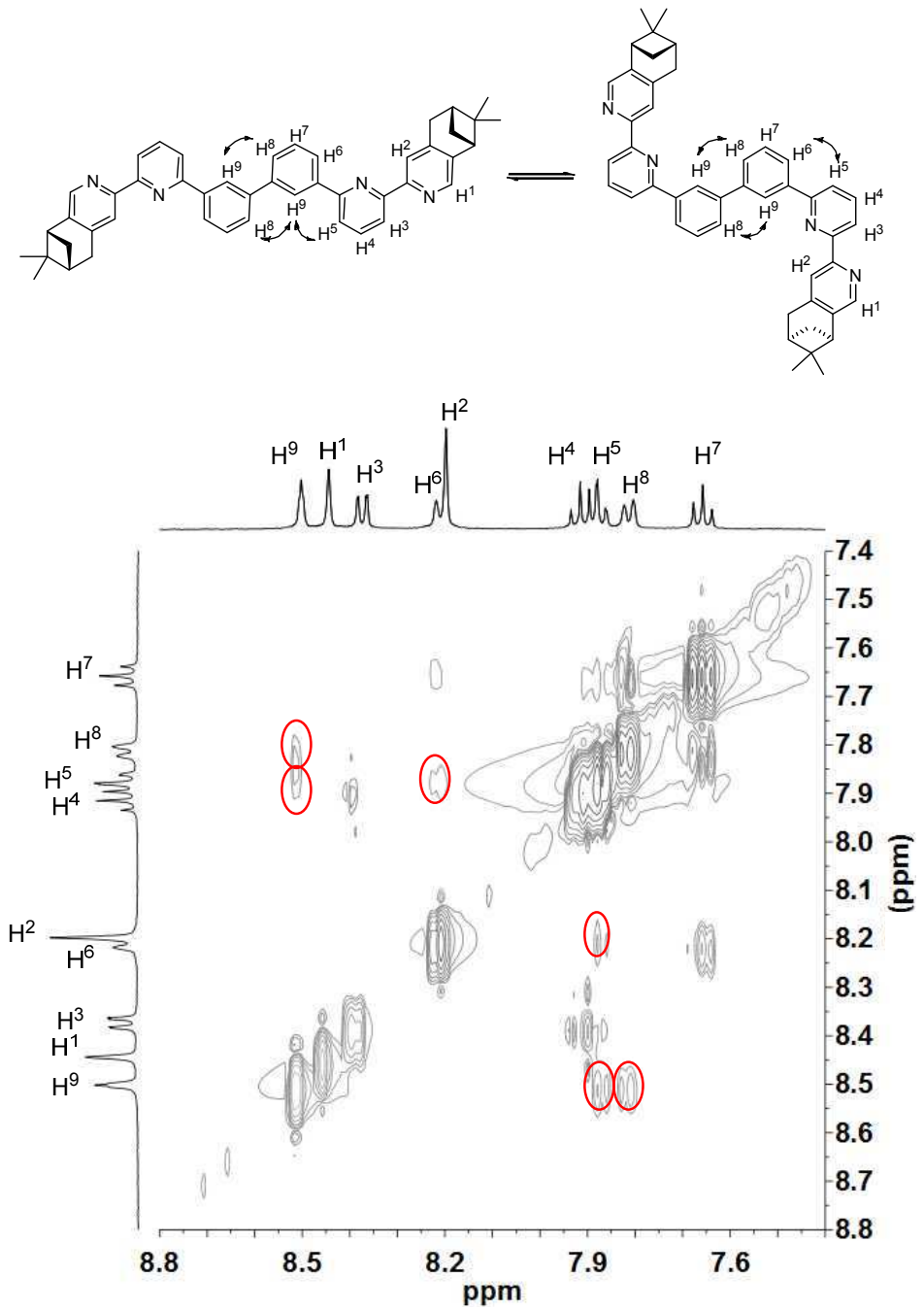

Figure 10 NOESY spectrum (400 MHz) of **L2** in CD_2Cl_2

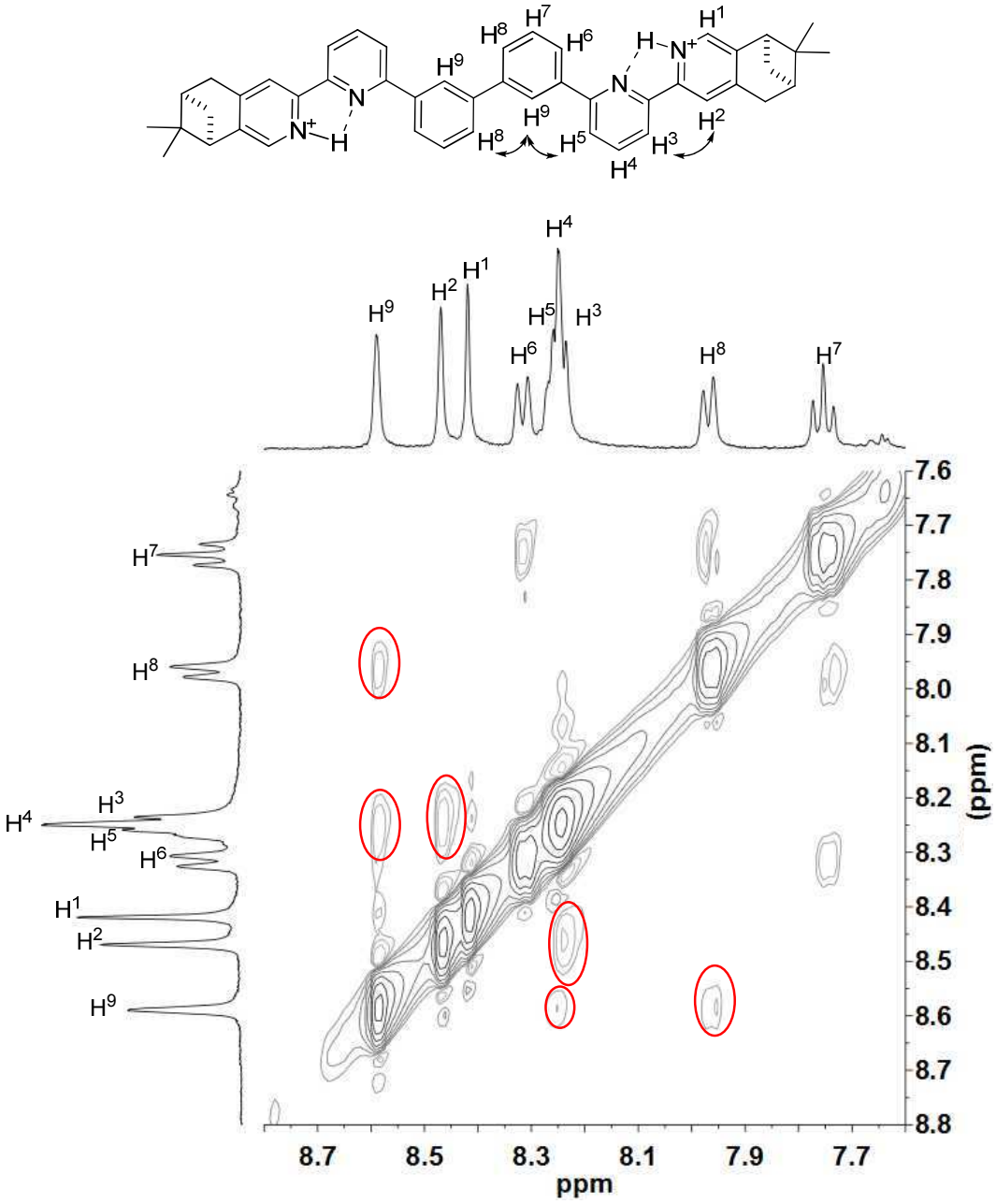

Figure 11 NOESY spectrum (400 MHz) of **L2** with addition of 2 equiv. of $HClO_4$ in CD_2Cl_2.

Low temperature ^{1}H NMR study

Apart from the upfield shift, broadening of signals of were also observed in NMR spectra of **L2–4** when $HClO_4$ was added. Variable temperature NMR experiments were then carried out to study the broadened signals. Figure 12–14 shows the effect of the temperature on the ^{1}H NMR signals. Figure 12 shows that the broadened signals of **L2** with 2 equiv. of $HClO_4$ become even broader when the sample is cooled to 0 °C. Further decrease in temperature leads to sharpening and splitting of the signals into two sets with one set significantly upfield shifted while the other set shifted downfield to chemical shift similar to that of the free ligand. Figure 13 shows the spectra obtained with **L3** and 1 equiv of $HClO_4$. Similar signals splitting is observed, but it starts at higher temperature of 0 °C. The most sharpened signals are observed at −40 °C. Figure 14 shows that signals of **L4** with 1 equiv $HClO_4$ also split into in two sets at 0 °C. The line-shape of the signals does not change much when the temperature is below −30 °C. These results suggest that the broadening of signals observed with **L2–4** and $HClO_4$ come from the exchange between an upfielded and a downfielded species. The differences in temperature in giving the splitting and change in line-shape of the signals suggest that the exchange rates are different. Analysis of the linewidth of the signals at temperature below coalescence give the free energy of activation for the exchange process[47,48] of 13.0, 13.4, and 14.0 kcalmol^{-1} for **L2**, **L3** and **L4**, respectively. By considering that the signals broadening and the upfield shift of signals occur at the same time, we believe that the exchanges involve monoprotonated species of **L2–4**.

After the variable temperature experiments, the NMR solutions were then characterized by ESI-MS at room temperature (Figure S1). The spectra show similar results to that of $HFeCl_4$ as both $[(\mathbf{L})_2H_2](ClO_4)^+$ and $[(\mathbf{L})H]^+$ were observed. These monoprotonated species can be considered monomer and dimer. We believe that the broadening of signals may be due to the exchange between the dimer and its monomeric form, and the stacking between the strands of the dimeric species is the reason that leads to anisotropic effects of the aromatic rings and upfield signals.

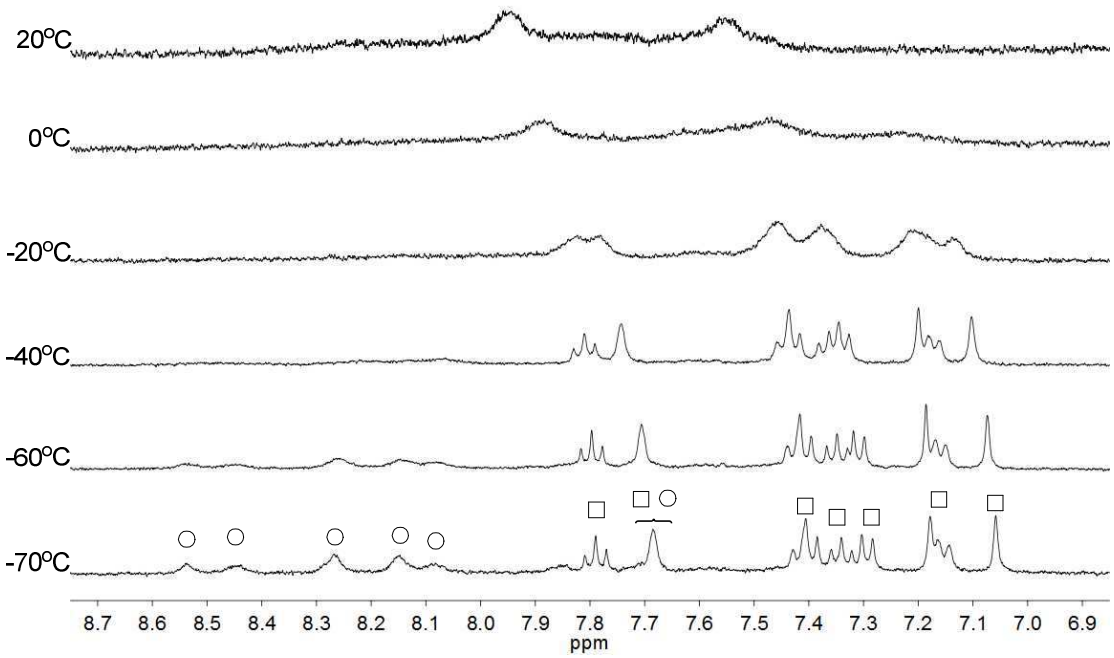

Figure 12 ^{1}H NMR spectra for **L2** (3×10^{-4} M) in CD_2Cl_2 with $HClO_4$ (2 equiv) at variable temperature. The species giving upfield and downfield signals are labelled □ and ○, respectively.

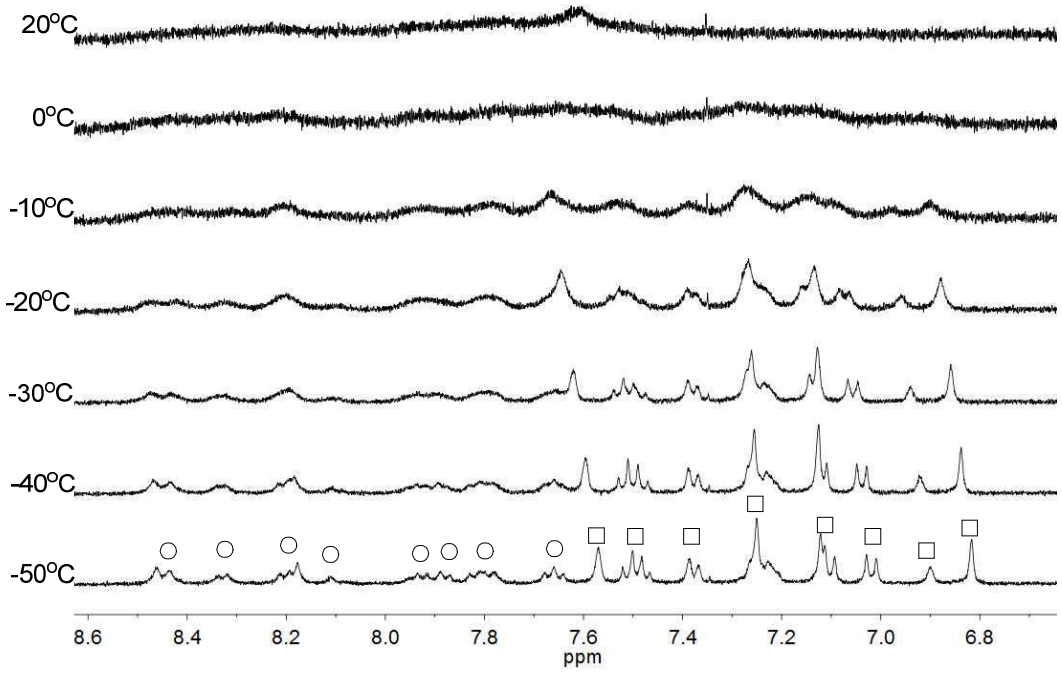

Figure 13 ^{1}H NMR spectra for **L3** (3×10^{-4} M) in CD_2Cl_2 with $HClO_4$ (1 equiv) at variable temperature. The species giving upfield and downfield signals are labelled

□ and ○, respectively.

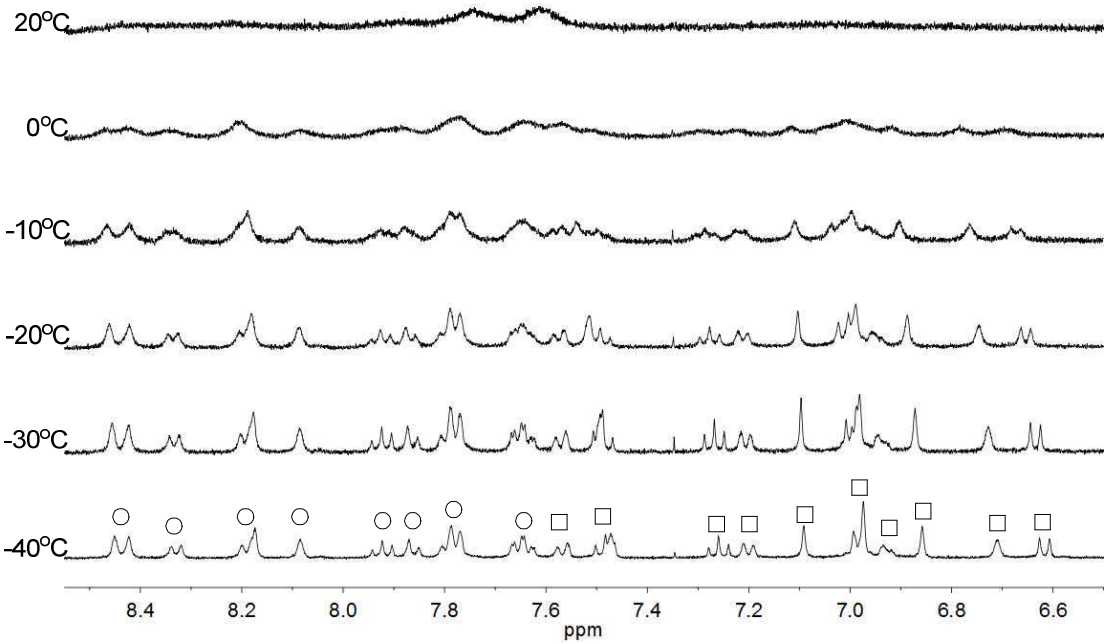

Figure 14 ^{1}H NMR spectra for **L4** (3×10^{-4} M) in CD_2Cl_2 with $HClO_4$ (1 equiv) at variable temperature. The species giving upfield and downfield signals are labelled □ and ○, respectively.

X-ray characterization

Single crystals suitable for X-ray analysis were obtained for the nonprotonated state of **L1**, the biprotonated state of **L4**, and the dimeric form of the monoprotonated **L2**. Crystals of **L1** were obtained by slowly evaporation of a diethyl ether solution. It is crystalized in a $P2_12_12_1$ space group. Figure 15 shows the ORTEP diagram. The pyridine rings adopt a transoid geometry and **L1** is not coplanar. Twisting is observed between the aromatic rings with the torsional angles between the pyridyl rings being 2.8° and 19.1°, and between the phenyl and pyridyl rings being 22.7° and 24.8°. The ligand is not long enough to have a complete helical turn, and there is no stacking interaction.

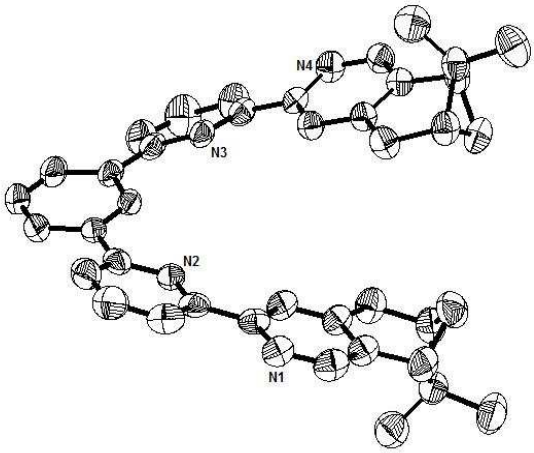

Figure 15 The ORTEP plot of crystal structure of **L1**. Hydrogen atoms are removed for clarity.

Single crystals of the biprotonated **L4** were obtained by ether diffusion into a methanol and chloroform solution of **L4** and $HFeCl_4$. The compound crystallized in a $P12_11$ space group. Although the mixture was prepared using a one to one molar ratio of **L4** and $HFeCl_4$, the biprotonated species of **L4** is a structure with a chloride and a tetrachloroferrate anions. The biprotonated **L4** coils up around the chloride ion to give two helical structures, the *P*- and *M*-helices, which are coexist in the crystal lattice. The structures of *P*- and *M*-helices are shown in figure 16a–d. Beside the methyl groups of the *P*-form is pointing towards the chloride and the methyl groups of the *M*-form is pointing away from the chloride, the structures of the two helices are very similar. In both structures, the pyridyl rings adopt a cisoid geometry and point toward the chloride ion. The coiling of **L4** comes from the twisting between the aromatic rings with most of it is contributed by the bridging phenyl rings. The dihedral angles between the phenyl rings are in the range 33.53–48.49°. The chloride anion has a close proximity with the terminal pyridine rings with N–H···Cl distances and angles in range 2.28–2.41 Å and 139.37–147.24°, respectively, which suggests the presence of hydrogen bonding. Although these species have helical structures, by considering that the anions are different, and the coexistence of the *P*- and *M*-form, these species are not related to the CD signals observed in the CD experiments. In addition, these biprotonated species shows that the tetraphenyl-bridged **L4** is long enough to give a complete helical turn, and there are stacking interactions between the terminal pyridine rings, however, no upfield signals shift is observed while the biprotonated species is formed in the ^{1}H NMR studies with $HClO_4$. It is not likely that this helical form of biprotonated **L4** is presented when only ClO_4^- anion is presented.

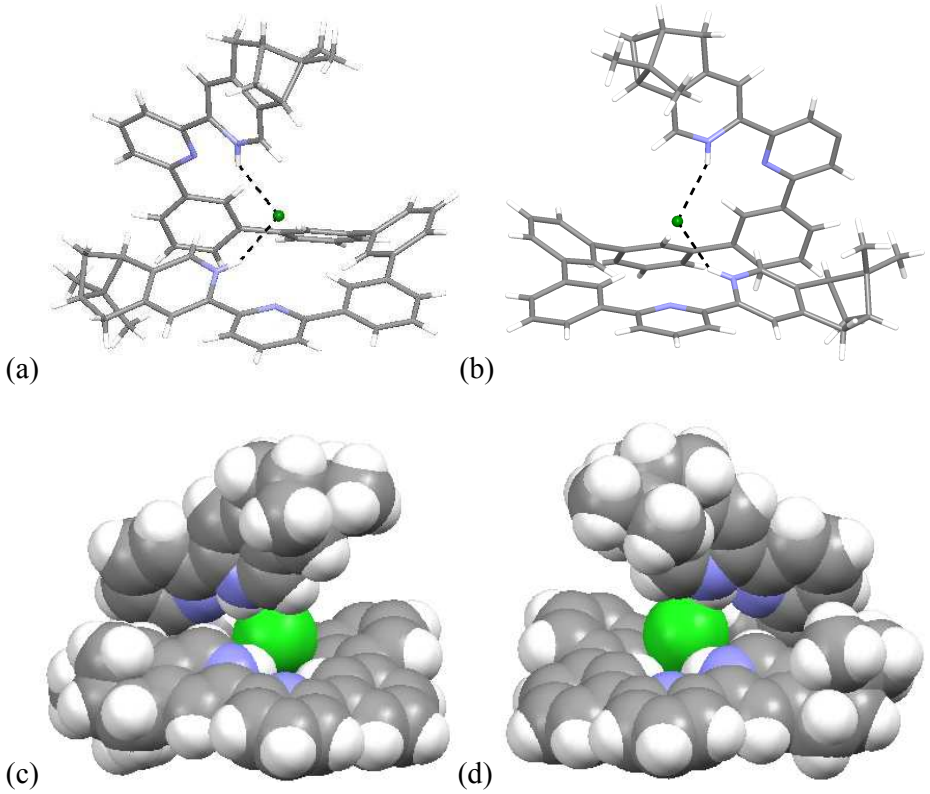

Figure 16 Capped stick drawing of X-ray crystal structure of (a) *P*- and (b) *M*-[(**L4**)H_2](Cl)($FeCl_4$). Dotted lines show hydrogen bonding with the chloride. The $FeCl_4^-$ ion is not shown for clearance. Figures (c) and (d) are the spacefilling model of *P*- and *M*-[(**L4**)H_2](Cl)($FeCl_4$) respectively.

Single crystals of the monoprotonated **L2** was obtained by ether diffusion into a solution of **L2** in the presence of 1 equiv of $HFeCl_4$. It crystallizes in a monoclinic *C*2 space group and it is a dimeric form of formula, [(**L2**)$_2H_2$]($FeCl_4$)$_2$. The structure, shown in figure 17, has syn pyridine rings and the two protonated strands twist around each other resulting in the double-stranded helical structure with *P*-helical chirality (Flack parameter = 0.026(7)). The two molecules of **L2** are held tightly together by intermolecular hydrogen bonding between the pyridinium proton of one strand and pyridine ring of the other strand. The N–H···N distances are 1.987 and 1.989 Å, and the angles N–H···N are 154.14 and 156.98°. The helix is also stabilized by π–π stacking interactions. There are extensive stacking interactions between the aromatic rings of the two molecules which start from the stacking of the pyridinium of one strand with the forth aromatic ring of the other, and extend along the whole ligand strand. Figure 18 shows the crystal lattice of [(**L2**)$_2H_2$]($FeCl_4$)$_2$. There are $FeCl_4^-$ anions surrounding the helix core. Some of the chloride atoms of the $FeCl_4^-$ are close to the aromatic hydrogens of the helix, and their distances and angles are summarized

in table 1. The C–H···Cl distances and angles are in the range 2.713–3.125 Å and 124.83–171.65° respectively. These results suggest the presence of the C–H···Cl hydrogen bonding interactions between the helix and $FeCl_4^-$ anions.[49–51] Figure 19 shows some of these interactions.

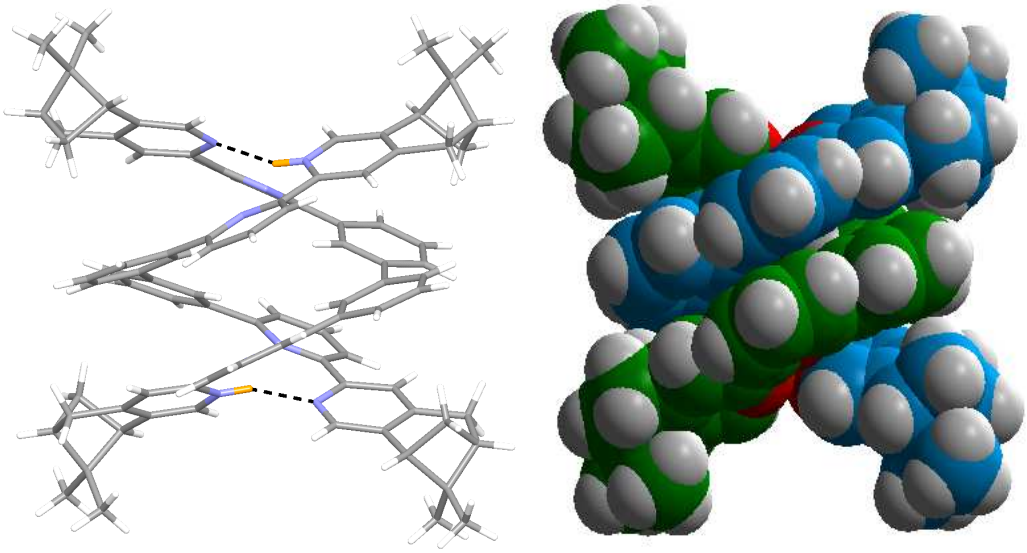

Figure 17 (a) Capped stick drawing of X-ray crystal structure of $[(\mathbf{L2})_2H_2](FeCl_4)_2$. Dotted lines show hydrogen bonding within the double helix. (b) Spacefilling model of X-ray crystal structure of $[(\mathbf{L2})_2H_2](FeCl_4)_2$.

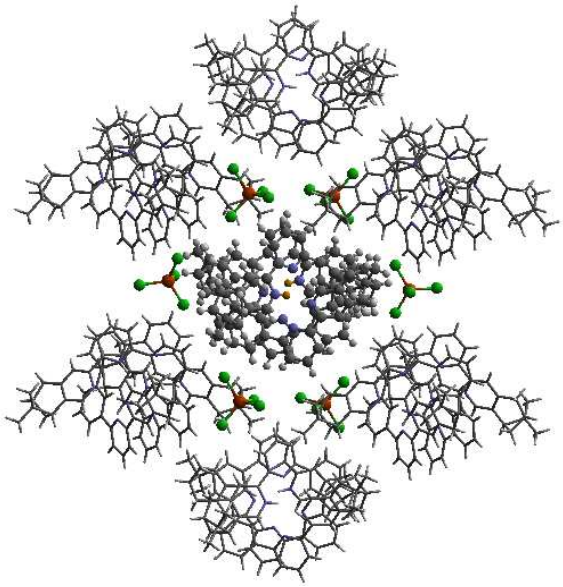

Figure 18 Crystal structure of $[(\mathbf{L2})_2H_2](FeCl_4)_2$ showing crystal packing and location of $FeCl_4^-$ anions surrounding the $[(\mathbf{L2})_2H_2]^{2+}$ core.

D–H···A	H···A/Å	D–H···A/°
N1–H1···N5	1.987	156.14
N8–H8···N4	1.989	154.98
C–H77···Cl1	3.036	165.66
C–H11···Cl2	2.713	162.04
C–H14···Cl3	3.119	124.83
C–H78···Cl5	2.906	139.35
C–H79···Cl6	3.097	136.80
C–H16···Cl7	3.057	132.81
C–H71···Cl6	3.042	128.50
C–H72···Cl6	3.090	126.66
C–H67···Cl8	3.031	137.48
C–H32···Cl1	2.880	162.13
C–H62···Cl3	2.996	136.51
C–H65···Cl4	2.747	128.67
C–H27···Cl8	2.994	171.65
C–H20···Cl4	3.125	152.81
C–H21···Cl4	2.768	166.47

Table 1 Hydrogen bonding parameters of $[(\mathbf{L2})_2H_2]^{2+}$ and surrounding $FeCl_4^-$ observed in X-ray crystal structure of $[(\mathbf{L2})_2H_2](FeCl_4)_2$.

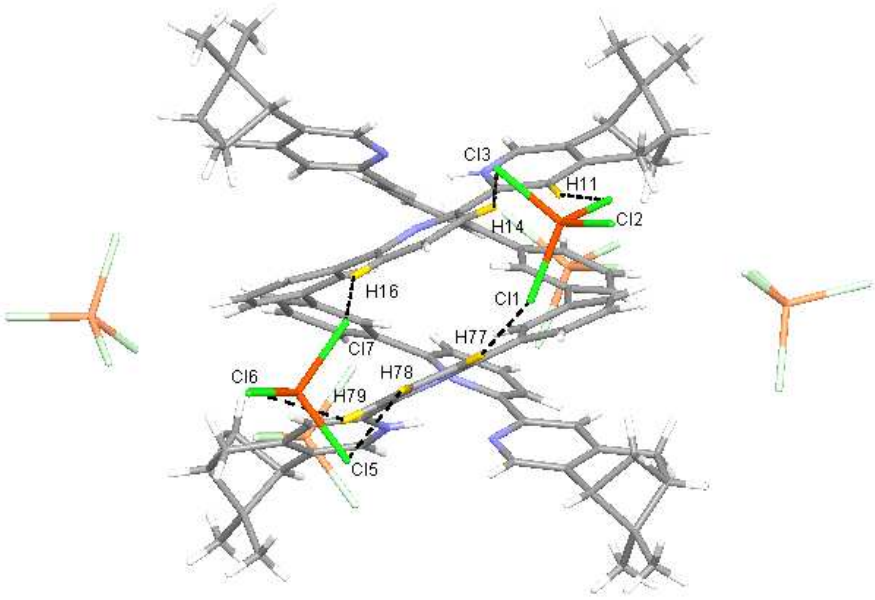

Figure 19 Crystal structure of $[(\mathbf{L2})_2H_2](FeCl_4)_2$ showing crystal packing and location of $FeCl_4^-$ anions surrounding $[(\mathbf{L2})_2H_2]^{2+}$ core. Dotted lines shows some of the hydrogen bonding between $FeCl_4^-$ and the helix

Solution state structure by DFT calculation

From the crystal structure of $[(\mathbf{L2})_2H_2](FeCl_4)_2$, we believe that a double-stranded helix is formed in solution when **L2** is monoprotonated in the presence of $FeCl_4^-$ or ClO_4^-, and the formation of the double helix is the origin the spectro-change observed in CD and NMR. The *P*-helical chirality of the $[(\mathbf{L2})_2H_2](FeCl_4)_2$ is consistent with the first positive CD signals observed in the CD spectra[52] which is similar to the spectra of the rigid Mn double-stranded helicates of **L2** and **L3**.[35] The extensive π–π stacking of the aromatic rings of the strands of the double-stranded helical structure which lead to anisotropic effect also agree well with the upfield signals observed in the NMR spectra. Considering the observation and results obtained with **L2**, **L3** and **L4** in the experiments, we believe that the monoprotonated form of triphenyl-bridged **L3** and tetraphenyl-bridged **L4** also form double-stranded helical structure. To show that this is the case and to have a better understanding to the helices in solution, DFT calculations were carried out on the monoprotonated species of **L2**, **L3** and **L4** using both the $FeCl_4^-$ and ClO_4^- anions.

Models of $[(\mathbf{L})_2H_2](FeCl_4)_2$ and $[(\mathbf{L})_2H_2](ClO_4)_2$ (**L** = **L2**–**4**) were first constructed, then their formation were investigated using theoretical DFT calculation at M06-2X level, with solvent effect taken account by the Polarizable Continuum Model. Figure 20 shows the calculation with the biphenyl-bridged **L2**. The calculation starts from protonation of **L2** and formation of the double-stranded helical core

$[(\mathbf{L2})_2H_2]^{2+}$. The formation of the helical core stabilizes the system by 164.4 and 107.8 kcalmol^{-1}, respectively, with $HFeCl_4$ and $HClO_4$. The energy different is the sum of dissociation of the $HFeCl_4$, protonation of **L2**, the stacking between the ligands and the pyridinium pyridine hydrogen bondings. Interactions between $[(\mathbf{L2})_2H_2]^{2+}$ with $FeCl_4^-$ and ClO_4^- anion further stabilize the system by 30.1 and 26.1 kcalmol^{-1}, respectively, which give $[(\mathbf{L2})_2H_2](FeCl_4)_2$ and $[(\mathbf{L2})_2H_2](ClO_4)_2$ with an overall stabilization 194.1 and 133.9 kcalmol^{-1}, respectively.

Similar calculations were carried out using **L3** and **L4** and the results are shown in figure 21 and 22. The results suggest that the formation of the double-stranded helices with **L3** and **L4** are also feasible, and also give additional information to the difference between these systems. In the presence of $HFeCl_4$, the formation of the double-stranded helical core $[(\mathbf{L})_2H_2]^{2+}$ with **L4** being the most stable (−173.4 kcalmol^{-1}), which is followed by **L3** (−172.1 kcalmol^{-1}), and then followed by **L2** (−164.4 kcalmol^{-1}). The same trend also occurs with $HClO_4$. These trends seem most likely due to the increase in the number of the bridging phenyl-rings of the ligands which increase the stacking interactions. Interactions between $[(\mathbf{L})_2H_2]^{2+}$ and $FeCl_4^-$ are in range −30.1 to −31.7 kcalmol^{-1}. With ClO_4^-, the interactions are in the range −25.3 to −28.3 kcalmol^{-1}. The $FeCl_4^-$ anion seems to have better stabilization than ClO_4^-. With the same anion, the differences in energy among **L2**−**4** suggest that the helices interact differently with different anions. The energy of −133.9 kcalmol^{-1} for $[(\mathbf{L2})_2H_2](ClO_4)_2$ is less stable than other helices which agrees quite well with the observations in the CD experiments.

The models of $[(\mathbf{L})_2H_2](FeCl_4)_2$ and $[(\mathbf{L})_2H_2](ClO_4)_2$ (**L** = **L2**–**4**) are shown in figure 23–25. Figure 23a shows the model of $[(\mathbf{L2})_2H_2](FeCl_4)_2$. The optimized geometry is in satisfactory agreement with its crystal structure, and the x-ray and calculated data are summarized in table 2. Beside the pyridinium N^+H and pyridine hydrogen bonding, there are C–H$\cdots$Cl type hydrogen bonding interactions between the $[(\mathbf{L2})_2H_2]^{2+}$ core and the two $FeCl_4^-$ anions very much similar to that observed in the X-ray structure. The bond distances and angles are summarized in table S1. The presence of C–H$\cdots$Cl hydrogen bondings are also confirmed by Atom in Molecules (AIM) analysis, and the results are shown in table S2. The $FeCl_4^-$ anions use three out of the four chloride atoms to hold the double-stranded helical structure by forming multi-centered hydrogen bonding to the protons on the first and the second aromatic rings of one strands, and the protons on the forth and firth aromatic rings of the other. The model of $[(\mathbf{L2})_2H_2](ClO_4)_2$ is shown in figure 21b. There are C–H$\cdots$O type hydrogen bonding interactions. The smaller ClO_4^- anions use three out of the four its oxygen atoms to form hydrogen bondings to the same aromatic protons on the backbone of both strands as $FeCl_4^-$ but with slightly different orientation. The data are

summarized in table S3 and S4.

X-ray structure of $[(\mathbf{L2})_2H_2](FeCl_4)_2$		Model of $[(\mathbf{L2})_2H_2](FeCl_4)_2$	
Atoms	Bond lengths or angles	Atoms	Bond lengths or angles
N1–H1···N5	1.987 Å	N89–H195···N194	1.890 Å
N1–H1···N5	156.14°	N89–H195···N194	157.00°
N8–H8···N4	1.989 Å	N181–H196···N92	1.894 Å
N8–H8···N4	154.98°	N181–H196···N92	156.48°
N1–C12–C13–N2	17.58°	N89–C26–C27–N90	23.83°
N2–C17–C18–C23	20.49°	N90–C34–C35–C43	12.87°
C23–C22–C24–C29	32.74°	C43–C42–C45–C53	29.67°
C29–C28–C30–N3	24.58°	C53–C52–C55–N91	20.82°
N3–C34–C35–N4	21.82°	N91–C62–C63N92	21.30°
N5–C58–C59–N6	24.04°	N181–C116–C119–N182	23.85°
N6–C63–C64–C69	22.81°	N182–C126–C127–C135	11.47°
C69–C68–C70–C75	34.24°	C135–C134–C137–C145	30.08°
C75–C74–C76–N7	13.29°	C145–C144–C147–N183	21.48°
N7–C80–C81–N8	20.35°	N183–C154–C155–N184	20.64°

Table 2 A summary of the selected bond lengths and angles of x-ray and calculated data of $[(\mathbf{L2})_2H_2](FeCl_4)_2$

Models with **L3** are shown in figure 22a and b. The stacking between the aromatic rings observed in $[(\mathbf{L3})_2H_2]^{2+}$ are different from $[(\mathbf{L2})_2H_2]^{2+}$. In the case of $[(\mathbf{L2})_2H_2]^{2+}$, the pyridinium of one strand stacks with the forth aromatic ring of the other, but the pyridinium stacks with the third aromatic ring in case of $[(\mathbf{L3})_2H_2]^{2+}$. Exterior hydrogen bindings between the helices and the anions are also observed. Data are summarized in table S5–8. Some differences are observed when comparing to **L2**. For **L3**, the $FeCl_4^-$ forms hydrogen bonds to the protons on the first and the second aromatic rings of one strands, but to the protons on the third and the forth aromatic rings of the other. In the presence of ClO_4^-, it forms hydrogen bonds to the same aromatic rings as $FeCl_4^-$ but with slightly different protons.

Models with **L4** are shown in figure 23a and b. The stacking observed in the helix of **L4** is different from **L2** and **L3**. The pyridinium of one strand stacks with the second aromatic ring of the other. The close proximity of the anions with the aromatic protons again suggest the presents of hydrogen bondings. The data are summarized in table S9–11. However, due to the size of the model of $[(\mathbf{L4})_2H_2](FeCl_4)_2$ excess the limit of the software, AIM analysis was only carried out on $[(\mathbf{L4})_2H_2](ClO_4)_2$. The

$FeCl_4^-$ forms hydrogen bonds to the protons on the first and the second aromatic rings of one strand, but to the protons on the third aromatic rings of the other, which is different from helix of **L2** and **L3**. The ClO_4^- also form hydrogen bonds to the same aromatic protons. Although the C–H···O and C–H···Cl hydrogen bonding are generally considered as weak hydrogen bonding,[49] the calculation results show that the sum of the interactions from the two anions are not weak (in range −30.1 to −31.7 $kcalmol^{-1}$ for $FeCl_4^-$, and −25.3 to −28.3 $kcalmol^{-1}$ for ClO_4^-), and is comparable to a strong hydrogen bond.[53] As shown in scheme 2, we believe that the formation of the double-stranded helix is a delicate combination of the two types of hydrogen bonding, the interior hydrogen bonding between pyridinium and pyridine, and the exterior hydrogen bonding between the core and anions.

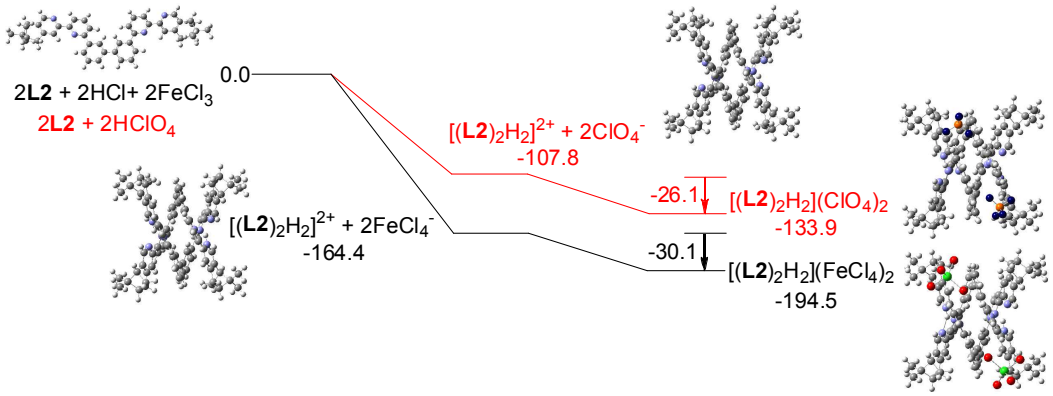

Figure 20 Energy profile of the formation of $[(\mathbf{L2})_2H_2](X)_2$ (X = ClO_4^- or $FeCl_4^-$) obtained by calculation at M06-2X/6-31G(d)/LANL2DZ with solvent effect. The red line indicates the formation of $[(\mathbf{L2})_2H_2](ClO_4)_2$ and black line indicates the formation of $[(\mathbf{L2})_2H_2](FeCl_4)_2$. The relative energy is given in kcalmol^{-1}.

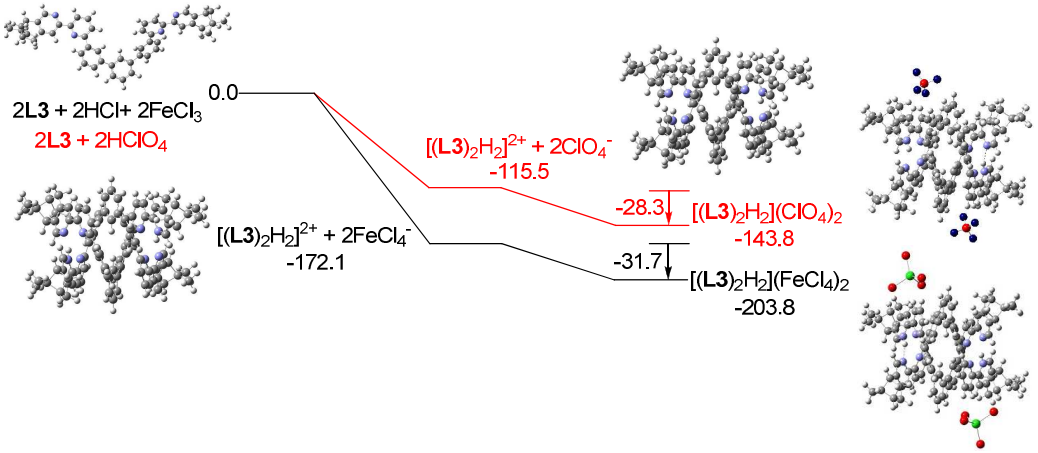

Figure 21 Energy profile of the formation of $[(\mathbf{L3})_2H_2](X)_2$ (X = ClO_4^- or $FeCl_4^-$) obtained by calculation at M06-2X/6-31G(d)/LANL2DZ with solvent effect. The red line indicates the formation of $[(\mathbf{L3})_2H_2](ClO_4)_2$ and black line indicates the formation of $[(\mathbf{L3})_2H_2](FeCl_4)_2$. The relative energy is given in kcalmol^{-1}.

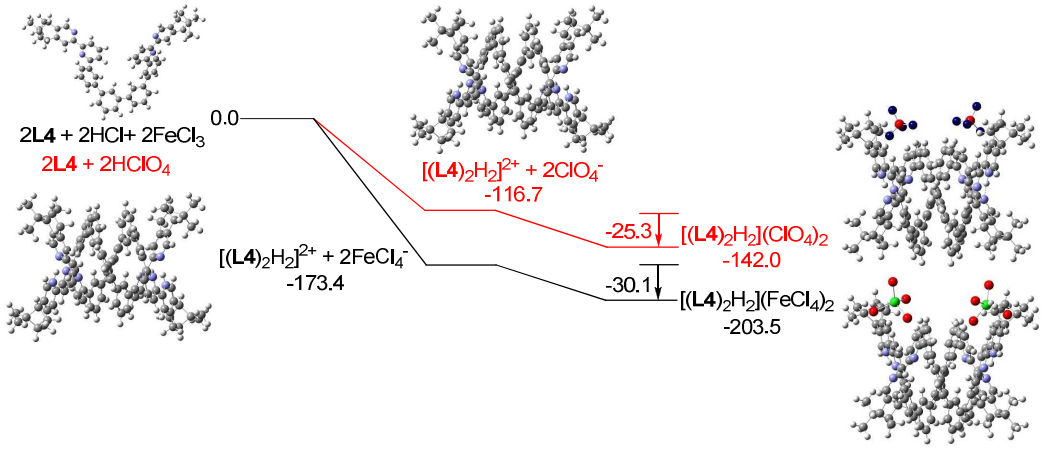

Figure 22 Energy profile of the formation of $[(\mathbf{L4})_2H_2](X)_2$ (X = ClO_4^- or $FeCl_4^-$) obtained by calculation at M06-2X/6-31G(d)/LANL2DZ with solvent effect. The red line indicates the formation of $[(\mathbf{L4})_2H_2](ClO_4)_2$ and black line indicates the formation of $[(\mathbf{L4})_2H_2](FeCl_4)_2$. The relative energy is given in $kcalmol^{-1}$.

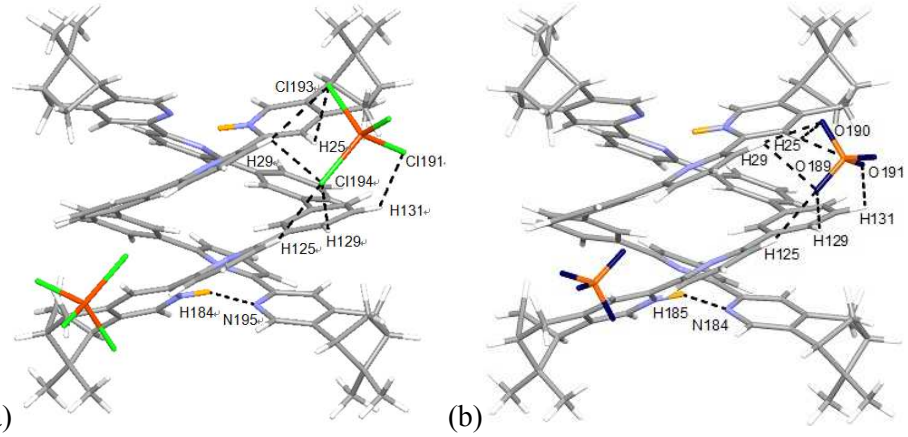

(a) (b)

Figure 23 Minimized energy model of (a) $[(\mathbf{L2})_2H_2](FeCl_4)_2$, and (b) $[(\mathbf{L2})_2H_2](ClO_4)_2$ obtained from theoretical calculation at M06-2X/6-31G(d)/LANL2DZ. Hydrogen bonding interactions are shown with dotted lines on only one of the anions for clearance.

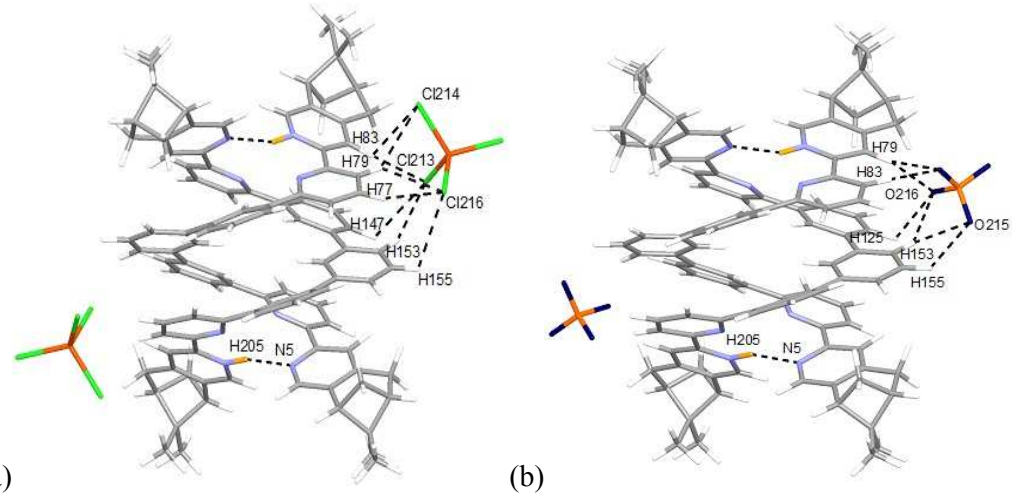

(a) (b)

Figure 24 Minimized energy model of (a) $[(\mathbf{L3})_2H_2](FeCl_4)_2$, and (b) $[(\mathbf{L3})_2H_2](ClO_4)_2$ obtained from theoretical calculation at M06-2X/6-31G(d)/LANL2DZ. Hydrogen bonding interactions are shown with dotted lines on only one of the anions for clearance.

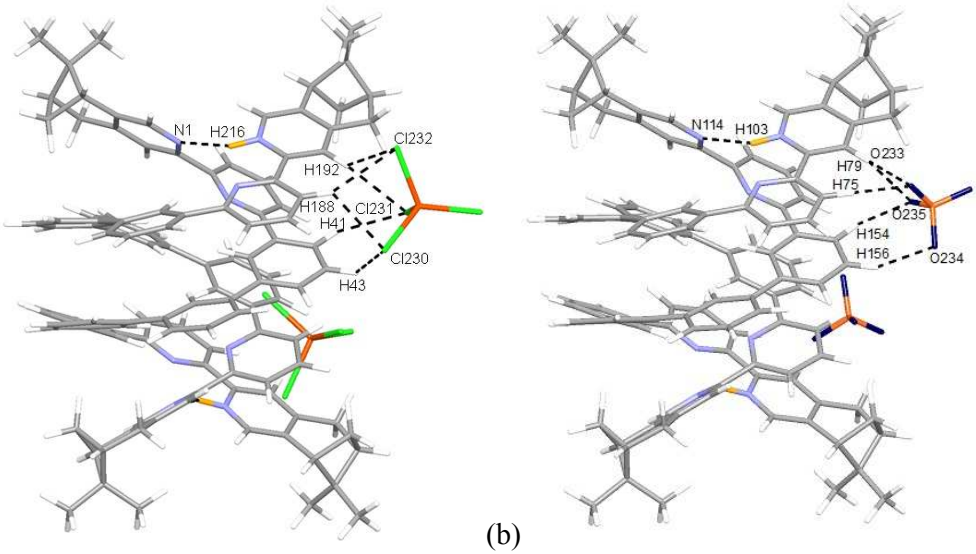

(a) (b)

Figure 25 Minimized energy model of (a) $[(\mathbf{L4})_2H_2](FeCl_4)_2$, and (b) $[(\mathbf{L4})_2H_2](ClO_4)_2$ obtained from theoretical calculation at M06-2X/6-31G(d)/LANL2DZ. Hydrogen bonding interactions are shown with dotted lines on only one of the anions for clearance.

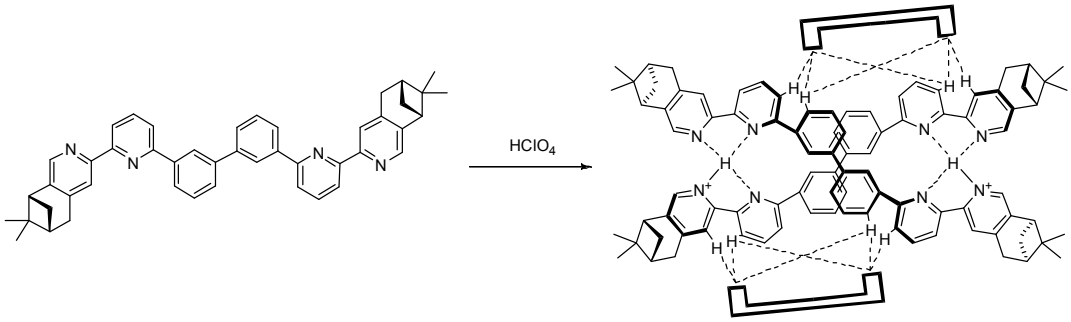

Scheme 2 Formation of hydrogen-bonded double-stranded helix $[(\mathbf{L2})_2H_2](ClO_4)_2$ with ClO_4^- anions represented by ⊓.

Reversibility of the formation of the hydrogen-bonded double helix

Since reversible interconversion between multistable states of a molecule in response to protonation is of interest,[54–56] we tried to see if **L2**–**4** can be developed into reversible interconverting systems with CD signal change by sequential addition of acid and base. With $HFeCl_4$ and NEt_3 as base, excess NEt_3 (5 equiv) is needed to turn off the CD signal, but addition of the $HFeCl_4$ cannot fully restore the original CD signal suggesting that the process is not reversible with $HFeCl_4$. However, with $HClO_4$, the results were quite different. Figure 26a shows the results of reaction of **L2** with $HClO_4$ and NEt_3. When $HClO_4$ is used, addition of NEt_3 turns the signal "off". Addition of another equiv of $HClO_4$ turns the signal "on" again restoring the CD

signal. This cycle can be repeated without the decrease in signal's intensity for at least four to five cycles. This on and off CD signal switching properties can be demonstrated by using **L3** and **L4** (figure 26b and c). The results suggest that these systems have potential to be developed as chiroptical switches.

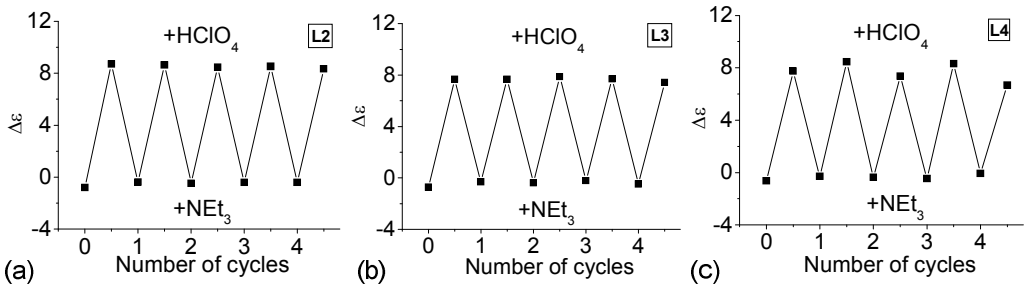

Figure 26 CD absorption at 334 nm of (a) **L2**, (b) **L3**, and (c) **L4,** with alternate addition of $HClO_4$ and NEt_3.

Conclusion

We have presented the synthesis of a series of chiral polyphenyl-bridged bis(2,2'-bipyridine) ligands. Protonation of the ligands give intense CD signals. The protonation processes were studied in detail by both CD and ^{1}H NMR. The results suggest that the CD signals come from monoprotonated species. X-ray crystal structures of free ligand and protonated ligands were obtained. The structure of the monoprotonated ligand shows that it is a double-stranded helix that is stabilized by a delicate combination of interior hydrogen bonds between the ligand strands and exterior hydrogen bonds between the helical core and anions. Theoretical DFT calculations on the formation of hydrogen-bonded double helices with the series of ligands were carried out. We believe that hydrogen-bonded double helices are formed upon monoprotonation of the ligands and they are stabile in solution as well. With perchlorate anion, the system can be interconverted between non-helical and helical states by addition and removal of proton, making it an on/off chiroptical switch. Further investigation of these properties for other applications line is now in progress.

Acknowledgment

The work described in this paper was supported by grants from the University Grants Committee of Hong Kong Special Adminstrative Region, China (Project No. [AoE/P-03/08] and CityU 7004018).

References

1) W. Saenger, *Principles of Nucleic Acid Structure*, Springer-Verlag, New York, 1999.
2) J.-M. Lehn, *Supramolecular Chemistry: Concepts and Perspectives*, VCH, Weinheims, 1995, section 9.3.
3) J. W. Steed, J. L. Atwood, *Supramolecular Chemistry*, John Wiley and Sons Ltd, Chichester, 2000, chapter 7.7.
4) S. Howson, P. Scott, *Dalton Trans.*, 2011, **40** 10268.
5) C. Piguet, M. Borkovec, J. Hamacek, K. Zeckert, *Coord. Chem. Rev.*, 2005, **249**, 705.
6) M. J. Hannon, L. J. Childs, *Supramol. Chem.*, **2004**, *16*, 7.
7) M. Albrecht, *Chem Rev.,* 2001, **101**, 3457.
8) C. Piguet, G. Bernardinlli, G. Hopfgartner, *Chem. Rev.*, 1997, **97**, 2005.
9) H. Ito, Y. Furusho, T. Hasegawa, E. Yashima, *J. Am. Chem. Soc.*, 2008, **130**, 14008.
10) Y. Tanaka, H. Katagiri, Y. Furusho, E. Yashima, *Angew. Chem. Int. Ed.*, 2005, **44**, 3867.
11) A. Stephenson, M. D. Ward, *RSC Advances*, 2012, **2**, 10844.
12) A. Stephenson, M. D. Ward, *Chem. Commun.*, 2012, **48**, 3605.
13) V. Vreshch, M. E. S. Moussa, B. Nohra, M. Srebro, N. Vanthuyne, C. Roussel, J. Autschbach, J. Crassous, C. Lescop, R. Réau, *Angew. Chem. Int. Ed.*, 2013, **52**, 1968.
14) V. E. Campbell, X. de Hatten, N. Delsuc, B. Kauffman, I. Huc, J. R. Nitschke, *Chem. Eur. J.*, 2009, **15**, 6138.
15) A. R. Stefankiewicz, M. Walesa, P. Jankowski, A. Ciesielski, V. Patroniak, M. Kubicki, Z. Hnatejko, J. M. Harrowfield, J.-M. Lehn, *Eur. J. Inorg. Chem.*, 2008, 2910.
16) E. C. Constable, M. J. Hannon, A. Martin, P. R. Raithby, *Polyhedron*, 1992, **11**, 2967.
17) R. Amemiya, M. Yamaguchi, *Chem. Rec.*, 2008, **8**, 116.
18) D. Haldar, H. Jiang, J.-M. Léger, I. Huc, *Angew. Chem. Int. Ed.*, 2006, **45**, 5483.
19) D. Haldar, H. Jiang, J.-M. Léger, I. Huc, *Tetrahedron*, 2007, **63**, 6322.
20) D. Haldar, C. Schmuck, *Chem. Soc. Rev.*, 2009, **38**, 363.

21) H.-B. Wang, B. P. Mudraboyina, J. A. Wisner, *Chem. Eur. J.*, 2012, **18**, 1322.
22) H. Yamada, K. Maeda, E. Yashima, *Chem. Eur. J.*, 2009, **15**, 6794.
23) H. Jiang, V. Maurizot, I. Huc, *Tetrahedron*, 2004, **60**, 10029.
24) V. Berl, I. Huc, R. G. Khoury, M. J. Krische, J.-M. Lehn, *Nature*, 2000, **407**, 720.
25) S. Mangani, M. Ferraroni, Natural Anion Receptors: Anion Recognition by Protein. In *Supramolecular Chemistry of Anions*, ed. A. Bianchi, K. Bowman-James, E. García-España, Wiley-VCH, New York, 1997.
26) *Comprehensive Coordination Chemistry II*, ed. J. A. McCleverty, T. J. Meyer, Elsevier, Oxford, 2004, volume 9.
27) M. S. Vivkers, P. D. Beer, *Chem. Soc. Rev.*, 2007, **36**, 211.
28) R. Vilar, *Angew. Chem. Int. Ed.*, 2003, **42**, 1460.
29) Y. Haketa, H. Maeda, *Chem. Eur. J.*, 2011, **17**, 1485.
30) S. J. Coles, J. G. Frey, P. A. Gale, M. B. hursthouse, M. E. Light, K. Navakhun, G. L. Thomas, *Chem. Commun.*, 2003, 568.
31) J. Keegan, P. E. Kruger, M. Nieuwenhuyzen, J. O,Brien, N. Martin, *Chem. Commun.*, 2001, 2192.
32) J. Sánchez-Quesada, C. Seel, P. Prados, J. de Mendoza, *J. Am. Chem. Soc.*, 1996, **118**, 277.
33) C. Dolain, V. Maurizot, I. Huc, *Angew. Chem. Int. Ed.*, 2003, **42**, 2738.
34) J. Cho, M. Tanaka, S. Sato, K. Kinbara, T. Aida, *J. Am. Chem. Soc.*, 2010, **132**, 13176.
35) K.-C. Sham, H.-L. Yeung, S.-M. Yiu, T.-C. Lau, H.-L. Kwong, *Dalton Trans.*, 2010, **39**, 9469.
36) H.-L. Yeung, W.-Y. Wong, C.-Y. Wong, H.-L. Kwong, *Inorg. Chem.*, 2009, **48**, 4108.
37) Y. Zhao, D. G. Truhlar, *Theor. Chem. Account.*, 2008, **120**, 215.
38) P. J. Hay, W. R. Wadt, *J. Chem. Phys.,* 1985, **82**, 270.
39) P. J. Hay, W. R. Wadt, *J. Chem. Phys.*, 1985, **82**, 284.
40) P. J. Hay, W. R. Wadt, *J. Chem. Phys.*, 1985, **82**, 299.
41) S. Miertuš, E. Scrocco, J. Tomasi, *Chem. Phys.*, 1981, **55**, 117.
42) S. Miertuš, J. Tomasi, *Chem. Phys.*, 1982, **65**, 239.
43) F. Biegler-König, *AIM2000*, University of Applied Sciences, Bielefeld, Germany.
44) $HFeCl_4$ was prepared in situ from HCl and $FeCl_3$
45) S. T. Howard, *J. Am. Chem. Soc.,* 1996, **118**, 10269.
46) S. J. Kavitha, K. Panchanaheswaran, J. N. Low, C. Glidewell, *Acta. Cryst.,* 2005, **C61**, o473.
47) J. Sandström, *Dynamic NMR spectroscopy*; Academic Press, London, 1982, chapter 6.

48) R. L. Paul, S. P. Argent, J. C. Jeffery, L. P. Hardling, J. M. Lynam, M. D. Ward, *Dalton Trans.*, 2004, 3453.
49) T. Steiner, *Angew. Chem. Int. Ed*., 2002, **41**, 48.
50) L. Brammer, E. A. Bruton, P. Sherwood, *Cryst. Growth Des.*, 2001, **1**, 277.
51) C. B. Aakeröy, T. A. Evans, K. R. Seddon, I. Pálinkó, *New. J. Chem.* 1999, 145.
52) M. Zieglar, A. von Zelewsky, *Coord. Chem. Rev.*, 1998, 257.
53) G. A. Jeffery, *An introduction to Hydrogen Bonding*, Oxford University Press, Oxford, 1997.
54) S. M. Landge, I. Aprahamian, *J. Am. Chem. Soc*., 2009, **131**, 18269.
55) I. Okamoto, M. Nabeta, Y. Hayakawa, N. Morita, T. Takeya, H. Masu, I. Azumaya, O. Tamura, *J. Am. Chem. Soc.*, 2007, **129**, 1892.
56) J. D. Badjić, V. Balzani, A. Credi, S. Silvi, J. F. Stoddart, *Science*, 2004, **303**, 1845.

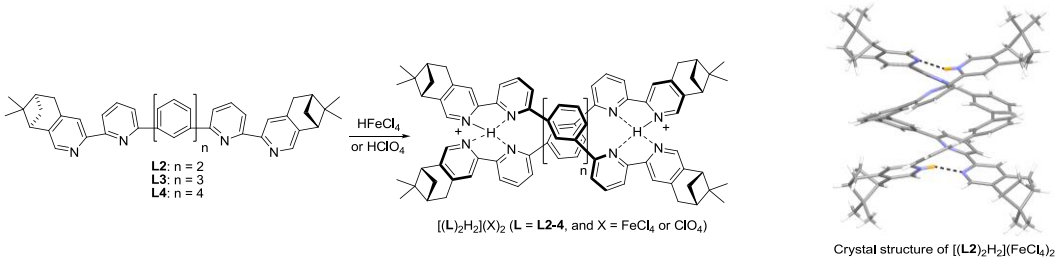

Chiral polyphenyl-bridged bis(2,2'-bipyridine) ligands **L2**-**4** give intense CD signals when protonated with tetrachloroferric acid or perchloric acid. X-ray crystal structures of $[(\mathbf{L2})_2H_2](FeCl_4)_2$ shows that a double-stranded helix stabilized by interior hydrogen bonding between the pyridinium N^+H and the pyridine N of another ligand strand, and exterior $CH\cdots Cl$ hydrogen bonding between $FeCl_4^-$ and the two ligand strands is formed. Theoretical DFT calculations show that such stabilization exists in solution.